Restoration of Blanket bogs; flood risk reduction and other ecosystem benefits

Annex 6. Flood risk modelling

Dave Milledge[3], Nick Odoni[3], Tim Allott[1], Martin Evans[1], Mike Pilkington[2], Jon Walker[2]

[1]Upland Environments Research Unit, Geography, University of Manchester, M13 9PL, UK; [2] Moors for the Future Partnership, Edale, S33 7ZA, UK; [3]Department of Geography, University of Durham, Durham, DH1 3LE, UK

Final report of the Making Space for Water project

Prepared for

By

Moors for the Future Partnership, 2015

Moors for the Future Partnership
The Moorland Centre,
Edale,
Hope Valley,
Derbyshire,
S33 7ZA, UK

T: 01629 816 579
E: research@peakdistrict.gov.uk
W: www.moorsforthefuture.org.uk

Suggested citation:
Milledge, D., Odoni, N., Allott, T., Evans, M., Pilkington, M. & Walker, J. (2015). *Annex 6: Flood risk modelling.* In Pilkington M.G. et al. (2015) *Restoration of Blanket bogs; flood risk reduction and other ecosystem benefits.* Final report of the Making Space for Water project: Moors for the Future Partnership, Edale.

CONTENTS

SUMMARY

1) This study had two aims: A1) to examine the impact of upstream interventions (gully blocking and re-vegetation) in the context of the larger catchment; A2) to use process based hydrological modelling at the micro-catchment scale to identify potential improvements to the effectiveness of interventions.

2) To address A1 we couple a Hydrological Response Unit (HRU) model with an Spatially Distributed Unit Hydrograph (SDUH) routing model. We use dynamic lumped models calibrated to each of the micro-catchment hydrographs using a Monte-Carlo-based uncertainty analysis to define the response of each HRU. We then propagate the runoff from these HRUs through the catchment using a 3 parameter SDUH model calibrated to the outlet hydrograph using the same MC-based uncertainty analysis. We simulate land management change over the gullied Kinder Plateau (12% of catchment area) by switching the runoff responses of the gullied HRU from that of a gullied system to that of re-vegetated and/or blocked gullies.

3) We find that if gully blocking and/or re-vegetation, reduces micro-catchment peak discharge by 20% there is a 7% probability that this will reduce outlet peak discharge by >4% and a 3% probability of reducing peak discharge by >8%. A larger discharge reduction of 40% increases these probabilities to 50% and a 6% respectively.

4) We conclude that restoration of 12% of the Ashop catchment by gully blocking and re-vegetation can be associated with an average reduction in peak discharge of 5% at the 9 km^2 scale.

5) To address A2, we focus on the effectiveness of wooden gully blocks. We use a simplified weir model to examine the effect of the number of weirs, their size and shape on the magnitude and timing of peak discharge from 5,000 - 7,000 m^2 micro-catchments during a gauged sequence of rain storms.

6) We find that gully block design can considerably improve efficacy of blocks in both reducing peak discharge and slowing the arrival time of the peak flow. From least to most effective these are: full brow, V-notch, rectangular slot, inverted V-notch, letter box slot. Within a given design the deeper the crest of the slot can be the more effective the weir will have. The smaller the slot (the narrower the crest, for a given slot depth), the more effective a weir will be up to an optimum, beyond which the weir overtops and all attenuation is lost. Weirs should therefore be optimised for the largest expected storm. Cascades of weirs increase attenuation but the 1st weir often reduces peak discharge considerably more than each additional weir. Cascades of weirs are more likely to perform well over a range of discharges than individual weirs.

1 UPSCALING THE IMPACT OF RESTORATION ON PEAK DISCHARGE

1.1 Introduction

There is considerable current interest in the impact of upstream land management on downstream flood risk. This relationship can be examined in several different ways. One approach that is attractive would be to develop a physically based model that can represent different land management activities, capture the hydrological behaviour of the different settings and be applied at the catchment scale. There have been a number of recent attempts to do this for upland peat catchments (Odoni and Lane, 2010; Ballard *et al.* 2012; Lane & Milledge 2012; Gao *et al.*, 2014). However, to date no attempt has been made to apply these models to the gullied Peak District peatlands, nor to their landscape-scale restoration through re-vegetation of bare peat and gully blocking. The challenge to modelling these systems is that such restoration has the potential to alter the system's hydrological function significantly through changes in runoff generation processes, runoff pathways and catchment storage. Existing models applied to these sub-catchments (OVERFLOW, Odoni and Lane, 2010; FLOWMAP, Lane and Milledge, 2012) were rejected as unsuitable following initial tests against observed hydrographs at the hectare scale. These models either failed to reproduce observed hydrograph characteristics or required un-physical behaviour in order to fit the model to the observations.

An alternative empirical approach would be to compare observed discharge at a location or locations downstream of the intervention. However, such approaches are limited by a lack of suitable discharge data, i.e. before and after intervention, and can only be used to examine historical scenarios. The MS4W project has taken a BACI strategy to examine the impact of gullies, gully blocking and re-vegetation on peak discharge from hectare scale micro-catchments. These observations suggest that: 1) gullied catchments have higher peak discharge per unit area and shorter lag-to-peak times than intact catchments; 2) re-vegetation reduces peak discharge and increases lag to peak; 3) gully blocking and re-vegetation together further reduce peak discharge and increase lag to peak (Annex 5, Section 4). While these findings suggest that gully blocking and re-vegetation can significantly reduce peak discharge at the hectare scale it is not clear what impact this will have on catchment scale discharge and downstream flood risk.

Here we take a simple modelling approach to upscale the observed changes in rainfall-runoff behaviour from micro-catchment to catchment scale (~9 km^2). We first calibrate a dynamic lumped model to each of the micro-catchment hydrographs representative of different hydrological response units (HRUs) in the catchment. We then propagate the runoff from these HRUs through the catchment using an spatially distributed unit hydrograph (SDUH) approach. Finally, we simulate land management change over the gullied Kinder Plateau (12% of catchment area) by switching the runoff responses of the gullied HRU from that of the gullied micro-catchment to that of re-vegetated and/or blocked micro-catchments.

1.2 Model Development

1.2.1 Lumped model for micro-catchment runoff

Qualitative description

The approach taken in this research to devise a model structure that allows the state variables and model parameters to be related to quantities that are, at least potentially, measurable in the field. In this way, it should be possible to link the behaviour of the state variables to each other so that runoff from the system (the peat upland micro-catchments) is predicted in a manner that is both realistic after model calibration, and also achieved without having to employ unrealistic values for the model parameters or allow unrealistic values to be modelled for the state variables.

The model structure conceived for this purpose, after some preliminary testing with proto "toy" model structures, comprises two state variables (Figure 1.1), the first, a volumetric store of water in the surface peat layer (presumed here to include mainly the acrotelm and upper layers of the catotelm), given the symbol *A*, and the second, a volumetric store of water in the channels and rills of the micro-catchment, given the symbol *Ch*. For convenience, the *A* store will be termed in this discussion the "acrotelm" even though it may include deeper peat layers. Similarly, the *Ch* store will be referred to as the "open flow" store as it is assumed to include all of the water in areas of open surface flow, whether in a properly formed channel or rill, or simply in open areas of peat linked in some way to the channels, or to rills flowing into the channels, and thence to the outlet of the site.

In the model, a volume of rain falling on a site is assumed to be absorbed first into the acrotelm store provided it has available capacity, that capacity denoted A_{cap}. Water is then assumed to flow from the acrotelm into the open flow store via a process likened to throughflow in a normal soil. Water in the open flow store is then routed to the outlet.

Under certain conditions, the capacity of the acrotelm may be reached. When this happens, any surplus volume of rain is routed direct to the open flow store, in a process similar to quickflow. It should be noted that the acrotelm is not therefore ascribed an infiltration capacity, so there is no limiting infiltration rate. Rather, the quickflow response is only dependent upon whether the acrotelm store has reached capacity and there is surplus rain volume to allocate to the other state variable.

Having provided a qualitative description of the model, the mathematical representation of these model relations may now be presented.

Mathematical formalisation of the model structure.

At any time, the acrotelm will contain a volume of water per unit area, *A* ($m^3\ m^{-2}$). There will also be a rate of increase in *A*, caused by rainfall (when it falls), and a decrease in *A*, caused by throughflow, which occurs all the time. The equation of state is therefore given by:

$$\frac{\partial A}{\partial t} = I - Q_t \qquad \text{(eq. 1)}$$

where *I* is the infiltration rate and Q_t the throughflow at any time instant. For discrete time steps, equation 1 becomes:

$$\Delta A|_{t_1}^{t_2} = \Delta t \times (I_{t,1} - Q_{t,1}) \quad \text{(eq. 2)}$$

where $\Delta A|_{t_1}^{t_2}$ is the change in the volume of water stored in the acrotelm during the period of time from t_1 to t_2, Δt is the length of the time step (equal to t_2 minus t_1), $I_{t,1}$ is the infiltration (from rain) at time t_1, and $Q_{t,1}$ is the throughflow at time t_1. The change in the volume is then added to the store, so we have:

$$A_{t,2=}A_{t,1} + \Delta A|_{t_1}^{t_2} \quad \text{(eq. 3)}$$

where $A_{t,1}$ and $A_{t,2}$ are the volumes stored in the acrotelm at times t_1 and t_2 respectively.

The infiltration during the time step depends upon the spare capacity of the acrotelm store. First, the notional addition to the store is calculated, V_{max}, equal to the rainfall rate (m s^{-1}) times the length of the time step. If this is equal to or less than the space capacity, all of the rainfall volume, V_{max}, is added to the acrotelm. However, if the capacity is less than the notional rain volume, only as much as the spare capacity is added to the acrotelm store and the excess is passed direct to the open flow store. Mathematically, this is represented as follows:

$$I_{t,1} = \begin{cases} k_R R \Delta t \ , if\ A_{cap} - A_{t,1} \geq V_{max} \\ \dfrac{A_{cap} - A_{t,1}}{\Delta t} \ , if A_{cap} - A_{t,1} < V_{max} \end{cases} \quad \text{(eq. 4)}$$

Surface flow can then be calculated using:

$$Q_s = k_R R - I \quad \text{(eq. 5)}$$

And the non-linear relationship between soil water storage (A) and throughflow discharge (Q_t) is calculated using:

$$Q_t = k_A \left(\frac{A}{A_{cap}}\right)^{N_A} A \quad \text{(eq. 6)}$$

Where: K_A and N_A are parameters for the non-linear storage discharge relationship. The water flowing out of the soil as throughflow enters the channel network. The changing volume of water in the channel network can be tracked using a second conservation equation.

$$\Delta V_{ch}|_{t_1}^{t_2} = \Delta t \times (Q_{t,1} - Q_{ch,1}) \quad \text{(eq. 7)}$$

The discharge of water from the channel network (Q_{ch}) is defined by its width (w), depth (d), and velocity (v):

$$Q_{ch} = w\ d\ v \quad \text{(eq. 8)}$$

As a result discharge depends on water depth and thus the degree of catchment saturation. This is represented in the model as a second storage discharge relationship derived using equation 8 above and the manning equation for wide shallow flows (i.e. $w>>d$) commonly used to represent channel flow:

$$v = \frac{1}{n}\ d^{\frac{2}{3}}\ s^{\frac{1}{2}} \quad \text{(eq. 9)}$$

To calculate discharge we substitute equation 9 into equation 8:

$$Q_{ch} = w\ \frac{1}{n}\ d^{\frac{5}{3}}\ s^{\frac{1}{2}} \quad \text{(eq. 10)}$$

Where: s is the water surface slope and n is the manning roughness coefficient. If we then assume: 1) that water surface slopes in the catchment are approximately equal to channel bed slopes,

uniform in space and constant in time; 2) that channel width at the outlet and the area of the channel network are constant in time; and 3) that water depth in the channel changes consistently across the channel network so that $d=V_{of}/A_{of}$ then equation 8 can be re-arranged and simplified to:

$$Q_{ch} = \frac{\langle w \rangle \langle s \rangle^{\frac{1}{2}}}{n} \left(\frac{V_{of}}{A_{of}}\right)^{\frac{5}{3}} = k_{ch} V_{of}^{\frac{5}{3}} \quad \text{(eq. 11)}$$

Where:

$$k_{ch} = \frac{\langle w \rangle \langle s \rangle^{\frac{1}{2}}}{n A_{of}^{\frac{5}{3}}} \quad \text{(eq. 12)}$$

And where: <w> is mean width, <s> is mean slope, A_{of} is the open flow area and V_{of} is the volume of water in open flow.

1.2.2 Routing micro-catchment runoff

To upscale from the micro-catchment scale we assumed that the observed rainfall runoff relationships at the micro-catchments were representative of those throughout the catchment. We split the catchment into 2 hydrological response units (HRUs): intact and gullied (Figure 1.2a). In each of the intervention scenarios we changed the hydrologic response of the entire gullied area, but only this area. We defined all of the Kinder Plateau as gullied peat and the rest of the catchment as intact peat, resulting in 12 % of the catchment being classified as gullied peat. We used the lumped rainfall-runoff models calibrated for each of the study micro-catchments to represent: intact, gullied, re-vegetated and blocked conditions. Since the discharge observations come from catchments of approximately ½ ha in area, we segmented the catchment into 1700 sub-catchments with a mean size of 0.49 ha (standard deviation 0.05 ha) using the isobasin tool in Whitebox GIS (Lindsay, 2014, Figure 1.2b).

We then routed the runoff from each sub-catchment to the catchment outlet using a spatially distributed unit hydrograph (SDUH) approach (e.g. Maidment, 1993; Olivera and Maidment, 1999; Du et al., 2009; Lane and Milledge, 2012), that uses the time to equilibrium approach of Saghafian and Julien (1995). To do this we made three assumptions: (1) a single continuous and time-invariant flow path within a storm event (e.g. Maidment et al., 1996); (2) a linear system response in which, at higher flows, travel times are independent of the amount of runoff being routed (e.g. Olivera and Maidment, 1999); and (3) independence of response where two locations share elements of the same flow path (e.g. Maidment et al., 1996).

To implement this routing model requires a travel time distribution to be constructed for each HRU. To do this, cells with a catchment area greater than 1 ha are assumed to contain channels and given a single characteristic channel velocity (V_{ch}); those with smaller catchment areas are assigned a single hillslope velocity (V_{hs}). These velocities combined with the flow path length in channels (L_{ch}, Figure 1.2c) and hillslopes (L_{hs}, Figure 1.2d) give the travel time (T_i) from the downstream boundary of each sub-catchment to the catchment outlet:

$$T_i = \frac{L_{chi}}{V_{ch}} + \frac{L_{hsi}}{V_{hs}} \quad \text{(eq. 13)}$$

where: T_i is the travel time for the pressure wave to propagate from the downstream boundary of subcatchment *i* to the catchment outlet [s], L_{chi} and L_{hsi} are the flow path lengths in channels and over hillslopes respectively from the downstream boundary of subcatchment *i* to the catchment outlet [m]; and V_{ch} and V_{hs} are the characteristic channel and overland flow velocities respectively [m s^{-1}].

We calculated the area weighted frequency distribution of travel times for the intact and gullied HRUs in 10 minute bins. These frequency distributions (Figure 1.3) show the catchment area (A*(t)*) that delivers water to the outlet within a given 10 minute timelag (*t*) since leaving the downstream boundary of a sub-catchment.

We applied the model to the same study period used to calibrate the lumped models (i.e. 10th to 31st December 2013) at 10 minute resolution. We chose to predict runoff from each HRU using the lumped models rather than the observed data in order to avoid the influence of rainfall variability between micro-catchments.

We tested four scenarios: pre-intervention, re-vegetation only, blocking and re-vegetation and pre-gullying. In each case there were only two HRUs, gullied and intact. The intact HRU always had the same runoff response as that from the intact micro-catchment. The four scenarios therefore differed only in the runoff response assigned to the gullied HRU, these are shown in Table 1.1.

To calculate the discharge *Q* at the catchment outlet we convolved the runoff time-series (R(t)) and travel time distribution (*A*(*t*)) for the intact and gullied HRUs with the runoff time series for the gullied HRU differing between scenarios:

$$Q = R_{intact}\, A_{intact} + R_{scenario}\, A_{gullied} \qquad \text{(eq. 14)}$$

where: *Q* [$m^3 s^{-1}$] is the discharge at the catchment outlet, R_{intact} is the runoff from the intact micro catchment [m s^{-1}], A_{intact} is the travel time distribution for the intact HRU [m^2], $A_{gullied}$ is the travel time distribution for the gullied HRU [m^2]; and $R_{scenario}$ is the runoff assigned to the gullied HRU [m s^{-1}] for a particular scenario (shown in Table 1.1).

Initial tests suggested that baseflow made up an important component of the observed discharge at the Upper Ashop gauge. To address this we modified the model to include a groundwater store, which received a constant fraction (*k*) of the runoff (*R*) in any timestep and contributed a constant discharge at the catchment outlet. The groundwater store was assumed to be in steady state over the modelled period (i.e. no net gain or loss of storage, $Q_{out} = \langle Q_{in} \rangle$).

1.2.3 Model calibration and uncertainty analysis

We focus upon undertaking model uncertainty analysis and model calibration with reference to the outlet discharge. The analysis is based on the assumption that the downstream flow gauge data, at both the micro-catchment and Upper Ashop catchment scale, provide a reliable time series of river discharge. We took a multi-step approach to model calibration, calibrating each of micro-catchment individually using the observed discharge at its downstream boundary and retaining the best 1% of model runs. We then applied these calibrated micro-catchment models as sub-components to the catchment model calibrating the three parameters for the SDUH using the observed discharge at the outlet of the Upper Ashop catchment.

In each case model parameters were subject to a Monte-Carlo-based uncertainty analysis. We chose this methodology because we expected that parameter interactions could condition model response significantly. We used this analysis for model calibration by using the objective functions discussed below to narrow the parameter ranges. The final scenario analysis was then performed using these narrowed parameter ranges.

First, we specified a parameter range on the basis of literature review and prior experience that encompassed the range of plausible parameter values. We then randomly sampled 10 000 times within these parameter ranges making no *a priori* assumptions about the possible distribution of parameter values within those ranges. The same set of parameter ranges was applied to all four micro-catchments to produce 40 000 model runs.

For each micro-catchment we ranked each parameter set for each objective function. Finally, we sought to identify the parameter values required for a calibrated model by looking at the intersection of optimized parameter ranges for each objective function. We identified the possible parameter range for a given objective function. We then cross-compared these parameter ranges and used this as the basis of a final calibrated parameter range.

Central to the calibration and uncertainty analysis, was selection of a set of objective functions to quantify the relationship between model predictions and field observations. In each case we consider two or three objective functions. The Nash–Sutcliffe efficiency (NSE) is commonly used as a measure of performance for rainfall runoff models. Its main problem is that it places equal emphasis on all observations, when the focus is high flows. We used it here as we considered that obtaining a generally robust hydrological representation was important. Second, we used the root mean square error in magnitude of predictions of the ten largest observed discharges since this measure recognizes the importance of flood flows without relying exclusively on the most extreme flood. Finally, for the calibration of the SDUH model at the catchment outlet we used the two objective functions above in combination with the root mean square error in timing of predictions of the ten largest observed discharges since this recognizes the importance of flood flow timings as well as magnitudes which are particularly important in constraining the velocity parameters in the SDUH.

1.3 Results

1.3.1 Lumped Model Micro-Catchment Runoff Results

Model Calibration

Optimum model parameters for each micro-catchment vary considerably. Figures 1.9–1.12 show a matrix of scatter plots where each point is the result of a model run from the MC-based uncertainty analysis. Model performance is plotted on the y-axis based on two metrics: the NSE (a general measure) and Peak RMSE (a peak focussed measure). Each column in the scatter matrix represents a different parameter in the model and in each case the x-axis shows the assigned parameter value for that run. The scatter in these plots reflects model equifinality (i.e. many different parameter combinations can result in the same model performance). However these plots also enable identification of optimum parameter sets. Pattern to the upper surface of a given scatter plot indicates that the model is sensitive to that parameter, peaks indicate that a parameter must assigned a value close to the x co-ordinate of the peak to achieve best model performance

independent of all other parameter values (e.g. A_{cap} = 0.05-0.1 m for the re-vegetated case, Figure 1.10). The points are coloured to show optimum performance for the different objective functions and their combination. The best 2% of runs in terms of NSE are coloured dark blue and the best 2% of runs in terms of Peak RMSE are coloured light blue. As a result blue points will always form a horizontal layer on the top of the scatter plot, dark blue for the first row which shows performance in terms of NSE, and light blue for the second row, which shows performance in terms of Peak RMSE. However, the distribution of light blue points in the first row and dark blue in the second row indicate the performance of points optimised for one objective function measured in terms of the other objective function. In some cases there is considerable overlap (e.g. Figure 1.9 where both sets of blue points sit near the top of the scatter plot). This indicates that very similar parameters are capable of optimising both peak RMSE and NSE and can be considered good general parameter sets. In others there is considerable difference (e.g. Figure 1.10), indicating that the parameters required to optimise one objective function do not optimise the other and general parameter sets will inevitably be a compromise. The red and magenta points represent different methods of combining the Objective functions by subsampling parameter sets optimised by one OF to find the best 50% of parameter sets in terms of the second OF. Red points reflect optimisation first by NSE then by Peak RMSE, magenta points reflect optimisation first by Peak RMSE then by NSE. Since our focus is on storm events, capturing peak discharge is particularly important so we chose the parameter sets optimised first by Peak RMSE then NSE for further analysis.

Calibrated hydrographs: site by site analysis

Calibrated model hydrographs generally (but not entirely) envelope the observed discharge (Figures 1.5–1.8) the model performs best for the intact catchment (Figure 1.5) and worst for the gullied catchment (Figure 1.6). In particular, in the gullied case, the predicted hydrograph peaks after the observed hydrograph for all 100 optimum parameter sets. This suggests that the model is unable to capture the extremely flashy rainfall runoff response in the gullied catchment. This is perhaps unsurprising since the observed hydrograph is displaying extremely flashy behaviour with the peak discharge occurring within the same 10 minute time window as peak rainfall. This observation has interesting implications for runoff generation and routing in gullied peat catchments. It suggests either: 1) that the soil store is very small in these catchments (consistent with the very small optimised A_{cap} in Figure 1.10); or 2) that quick flow across the majority of the catchment is not saturation excess overland flow. Water table observations in gullied catchments suggest a considerable volume of available storage (Allot *et al.*, 2009) and water table heights measured in this gullied micro-catchment are ~198-568 mm (Annex 5, Section 2), implying that the second explanation is more likely. Other candidates for quick flow are: rapid subsurface flow in soil pipes or infiltration excess overland flow (OLF). While infiltration excess OLF is unusual for peat catchments (Holden *et al.*, 2001) there is some support for it in these disturbed systems (Goulsbra, 2010). Rapid subsurface flow in soil pipes has been suggested as the dominant quick flow mechanism in peat catchments (Holden and Burt), but this would require very rapid infiltration, even if subsequent pipe flow velocities were quite fast. This coupled with the observed attenuation in micro-catchment peak discharge suggests that OLF of some form is likely to be an important quick flow component.

Calibrated hydrographs: site comparison

Applying the model parameterised using the optimum 1% of parameter sets (from Peak RMSE followed by NSE optimisation) for each of the micro catchments results in significant differences in modelled run-off between micro-catchments (Figure 1.14A). When these hydrographs are compared with the observed run-off for the micro-catchments (Figure 1.13) the largest peak in the record is well represented (compare Figures 1.13(b) with 1.14A(b)) and both the observed and modelled hydrographs show the same order (in terms of largest to smallest peak discharge). The second largest peak is less well represented with a much larger than observed difference between gullied and re-vegetated cases and a much smaller than observed difference between intact and re-vegetated and gully blocked cases (compare Figures 1.13(c) with 1.14A(c)). This suggests that the largest storm is the best candidate for subsequent upscaling analysis since it is most effectively reproduced by the lumped models.

Applying the trained models to simulate intervention scenarios for a single catchment

The observed rainfall records from the micro-catchments suggest that some of the differences in runoff may be due to rainfall differences. The gullied site appears to have consistently highest rainfall and the intact site consistently lowest rainfall. These differences can be accounted for by running the sub-catchment models for a single rainfall hyetograph (Figure 1.14B). Here we show results using rainfall from the gullied case similar model behaviour is produced using the hyetographs of the other micro-catchments (not shown). While it is possible that the difference in rainfall reflects a bias in the rainfall data we will assume that this is not the case and instead that this difference is a true reflection of rainfall differences in the storms in question (this is a conservative assumption).

1.3.2 Upscaling Results

Model Calibration

The three parameters of the SDUH model were calibrated by comparing predicted and observed discharge over the study period at the Upper Ashop gauge. We used three objective functions: Nash-Sutcliffe efficiency (general fit, low flow focus); Root Mean Square Error of discharge for the 10 largest peaks in the record (high flow focus); and Root Mean Square Error of timing for the 10 largest peaks in the record (high flow focus). The timing objective function was added since timing is particularly sensitive to the two velocity parameters in the model.

We take a similar approach to that at the micro-catchments for calibration, combining the Objective Functions. First we sample the full parameter set for the best (4%) of parameters in terms of one OF, then subsample this set to find the best 50% of the set in terms of the second OF and finally subsample this new set to find the best 50% of the sets in terms of a third OF. We sample first by Peak RMSE, then by NSE and finally by Timing RMSE. Blue points in Figure 1.16 reflect the intermediate set optimised by Peak RMSE then by NSE, red points reflect the final set, optimised by Timing RMSE. Optimum model performances require channel velocities in the range 1-1.9 m/s, overland flow velocities in the range 0.01-0.1 m/s and a baseflow fraction in the range 0.3-0.55.

Peak discharge at the catchment outlet follows the same pattern as for the mini-catchments. The discharge time series contains 15 peak flow events, including three large events, where the unit

discharge is more than 0.25 m/s (Figure 1.15). The modelled hydrographs peak with a similar magnitude and at a similar time to the observed, though there remains considerable error in the magnitude of peak discharge and the rising limb is generally slightly gentler than observed. The second largest storm (Figure 1.15(c)) is slightly better represented than the largest storm (Figure 1.15(b)), where the model underestimates the peak discharge and almost completely misses a second peak on the falling limb of the first.

Downstream scenario results

Here we compare the downstream consequences of modification to the gullied Kinder Plateau (12% of the study catchment). We run the model 1000 simulations randomly sampling from the optimum parameter sets for each of the lumped HRU models and for the SDUH model. In each case we run the model under four scenarios: pre-intervention, re-vegetated, blocked and re-vegetated, and a scenario representing the behaviour of the system prior to gullying (labelled 'intact). We keep track of the difference between the pre- and post-intervention peak discharges for the 15 largest storms in the study period for both the micro-catchment hydrographs and the full study catchment hydrograph. This enables us to report: 1) the cumulative frequency distribution (CDF) of peak discharge change for the full sample; 2) the CDF of peak discharge change for a subset of the largest storms; 3) the relationship between storm size and discharge change (to assess whether the effect changes with storm size); and 4) the relationship between peak discharge reduction at the micro-catchment scale and that at the full catchment scale.

Figure 1.17 shows the cumulative frequency of fractional change in discharge under each of these scenarios relative to pre-intervention discharge for the 15 largest storms in the study period based on 1000 model runs using randomly sampled parameters from calibrated parameter sets. This can be interpreted as the probability that the peak discharge will be reduced by a fraction less than or equal to the x-axis value. Re-vegetation alone results in the smallest reduction in peak flow, with only 30% of runs resulting in peak flow reductions >5% and ~15% of runs resulting in an increase rather than decrease in peak flow. Re-vegetation and gully blocking together results in the largest peak flow reductions, with 50% of runs resulting in reductions > 5% and 15% of runs resulting in reductions >10%. The intact scenario sits between the blocked and re-vegetated scenario and that for re-vegetation alone. For both blocked and intact scenarios ~10% of runs result in an increase rather than reduction in peak flow, but <3% of runs result in an increase of >5%.

Figure 1.17 can also be used to establish the average (median) reduction in peak discharge over 15 storms and 1000 parameter sets for each of the restoration scenarios. The median fractional discharge reductions are: 0.025, 0.04 and 0.05 respectively for the re-vegetated, intact and gully blocked and re-vegetated scenarios. These results suggest that restoration of 12% of the Upper Ashop catchment by gully blocking and re-vegetation can be associated with an average reduction in peak discharge of 5% at the outlet of the Upper Ashop and re-vegetation alone with an average reduction of 2.5%.

The fine lines in Figure 1.17 show CDFs for individual storms, they show that there is considerable variability in the impact of interventions between storms. While in most storms an intervention (e.g. blocking and re-vegetation) results in discharge reduction for more than 90% of the model runs, in one of the storms during the study period intervention results in increased rather than reduced discharge for more than 90% for model runs.

Figure 1.18 shows the cumulative frequency of fractional change in discharge relative to pre-intervention discharge for the 3 largest storms in the study period. These are likely to be the storms of most concern in terms of flood risk. Peak 1 is the largest discharge in the study period, peaks 2 and 3 are very similar though peak 3 is generally slightly larger than peak 2. Re-vegetation alone results in a modest reduction in peak discharge for peaks 1 and 2 with a median reduction of 1.5% and 2.2% respectively but a generally larger reduction (median = 5%) for peak 3. Re-vegetation with or without gully blocking rarely results in an increase in peak discharge (<10% of runs) and no runs result in an increase of more than 2%. In the blocked and re-vegetated scenario 40% of runs result in discharge reductions >4% for peaks 1 & 2. However, only 20% of runs result in discharge reductions > 4% for peak 3. There is considerable difference in the impact of intervention between storms.

The intact (pre gully) scenario is less consistent between storms than the other scenarios and has a much wider spread to the changes in outlet discharge. For Peak 2 the intact scenario more than 50% of runs result in more than 9% reduction in peak discharge. However, for Peak 1 more than 25% of runs result in an increase in peak discharge (Figure 1.18).

Figure 1.19 shows that there is no consistent trend in discharge reduction with storm size (peak discharge) for any of the scenarios. This suggests that across the range of storm sizes tested here the impact of upstream interventions does not change systematically with storm size. However, Figures 1.17–1.19 all show that there is considerable variability in discharge reduction both between storms and within storms.

Some of the within storm variability may reflect the parameter sets, leading to differences in predicted micro-catchment discharge before and after intervention that are not consistent with the observations detailed in Annex 5 (Section 4). To account for this we now consider the effect that the fractional difference in micro-catchment discharge has on the fractional difference in outlet discharge.

Figure 1.21 shows that there is an upper limit to the change in outlet discharge that can be expected for a given change in micro catchment discharge. This upper limit follows broadly the same trend for re-vegetation, gully blocking and re-vegetation and the intact case. In each case the gradient of the upper limit is ~1/8 i.e. downstream discharge is reduced at a rate of ~0.125 percentage points per percentage point discharge reduction at the micro-catchment. This is interesting given that 12% of the upper Ashop catchment has been modified. However, further work is required to establish the extent to which the gradient of this upper limit is related to the areal coverage of intervention.

The main difference between the three interventions is their x-axis location (i.e. the fractional change in micro-catchment discharge associated with each). Very few of the intact or blocking and re-vegetation runs result in fractional changes of <0.2 at the micro-catchment scale, whereas re-vegetation alone results in fractional changes of zero or even increases in peak discharge. The y-intercept of the upper limit to discharge reduction is non-zero (Figure 1.21) so that even in the absence of reduction in micro-catchment discharge there is a reduction in outlet peak discharge. This is likely to reflect changes to the timing of the peak and to the form of the hydrograph at the modified sites. It indicates that it is not only the change in peak discharge but also timing that is important in attenuating discharge and reducing downstream flood risk. Figure 1.20 shows that the behaviour of the largest three storms is broadly consistent with that of all storms shown in Figure 1.21.

These results suggest that reducing peak discharge by 40% over 12% of the Upper Ashop catchment should result in a discharge reduction of 0-13% at the outlet. Figure 1.22 shows the likelihood of a particular reduction in, outlet peak discharge (y-axis) given a particular reduction in peak discharge at the micro-catchment scale (x-axis). These results suggest that for gully blocking and re-vegetation over 12% of the Upper Ashop catchment, reducing peak discharge by 40% has a 10% probability of increasing outlet peak discharge, a 50% probability of reducing peak discharge by >4% and a 6% probability of reducing peak discharge by >8%. If gully blocking and re-vegetation were to have a more modest impact reducing peak discharge by 20% over the same area has a 17% probability of increasing outlet peak discharge, a 7% probability of reducing peak discharge by >5% and a 3% probability of reducing peak discharge by >8% (Figure 1.22).

1.4 Key results: Discharge upscaling

1. Restoration of 12% of the Upper Ashop catchment by gully blocking and re-vegetation can be associated with an average reduction in peak discharge of 5% at the 9 km^2 scale and re-vegetation alone with an average reduction of 2.5%.
2. Restoration by gully blocking and re-vegetation can result in reduction in peak discharge of up to 12% and re-vegetation alone a reduction of up to 8%.
3. The intact scenario was designed to provide some indication of the impact of gullying on downstream discharge. However, the results are too variable to draw strong conclusions from this exercise.
4. The results are sensitive to both micro-catchment and routing model parameters with discharge reductions in each case varying from the maximum values quoted here to no change or even small discharge increases depending on the parameter combinations.
5. The magnitude of discharge change under different scenarios does not vary systematically with storm size (i.e. interventions are not more or less effective in larger storms). However, different storms with the study period did result in variability in discharge change.
6. For a given change in micro-catchment discharge the outlet discharge change ranges from 0 to an upper limit that increases with micro-catchment discharge reduction with a slope ~0.12, and an intercept of ~3%, for both re-vegetation alone and gully blocking and re-vegetation.
7. If gully blocking and/or re-vegetation, reduces micro-catchment peak discharge by 20% this has a 7% probability of reducing outlet peak discharge by >4% and a 3% probability of reducing peak discharge by >8%.
8. If gully blocking and/or re-vegetation, reduces micro-catchment peak discharge by 40% this has a 50% probability of reducing outlet peak discharge by >4% and a 6% probability of reducing peak discharge by >8%.

1.5 Figures

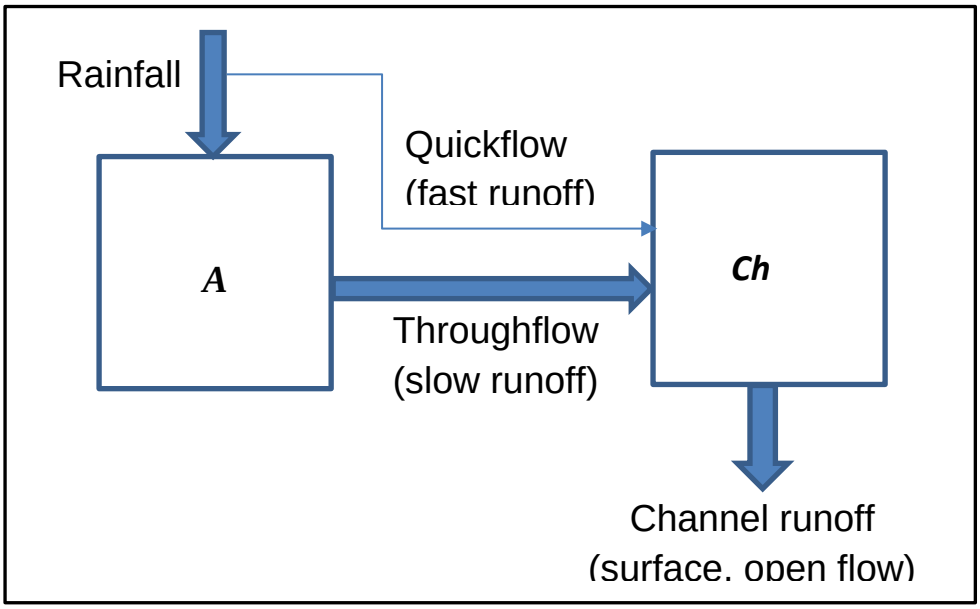

Figure 1.1: simple, schematic diagram of the hydrological model, showing the state variables and flow paths.

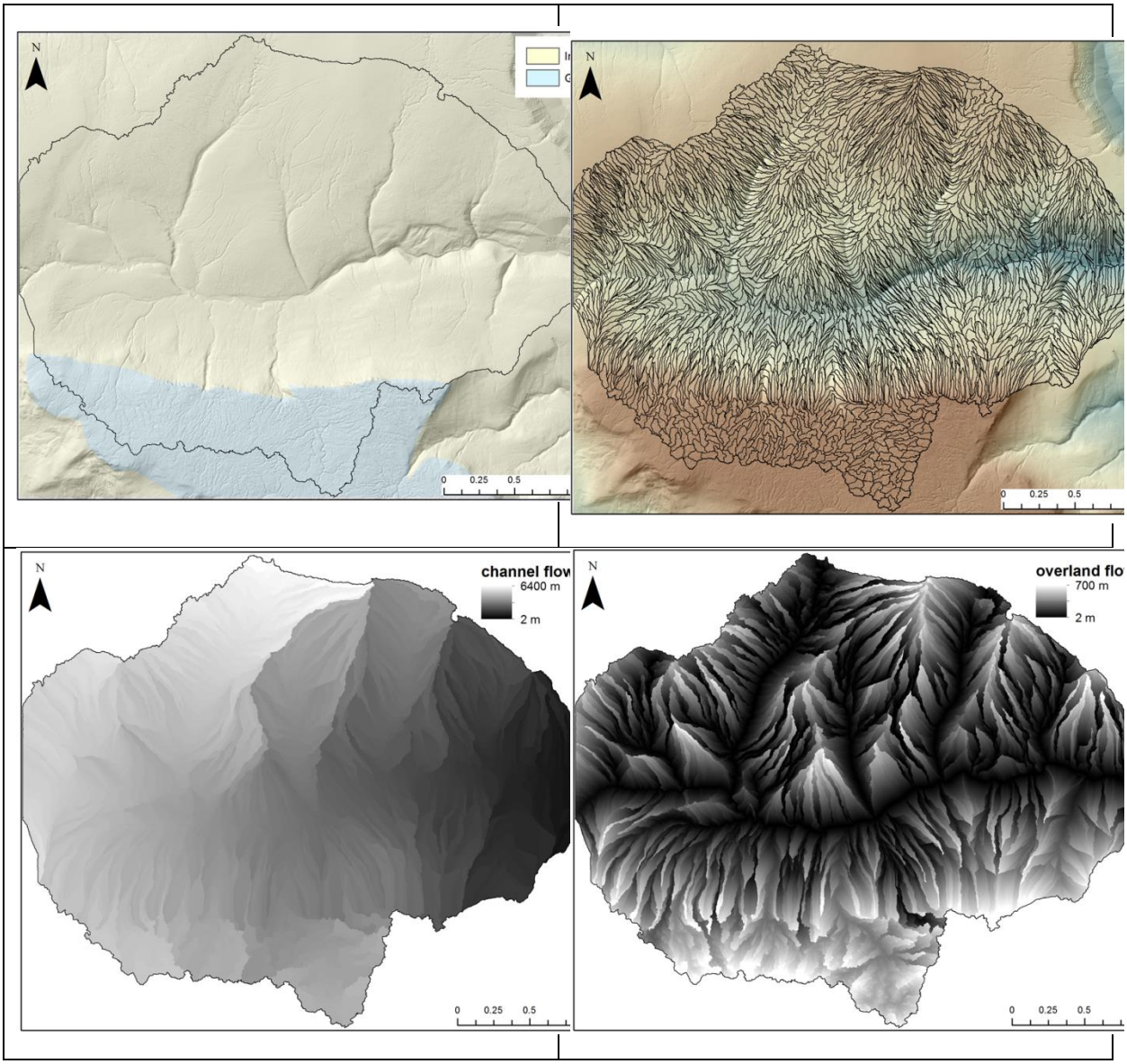

Figure 1.2: maps illustrating processing steps: a) the intact and gullied hydrological response units; b) the outlines of the 0.5 ha isobasins that make up the catchment; c) the length of channel from each point in the catchment to the outlet; and d) the length of hillslope flow path from each point in the catchment to the outlet.

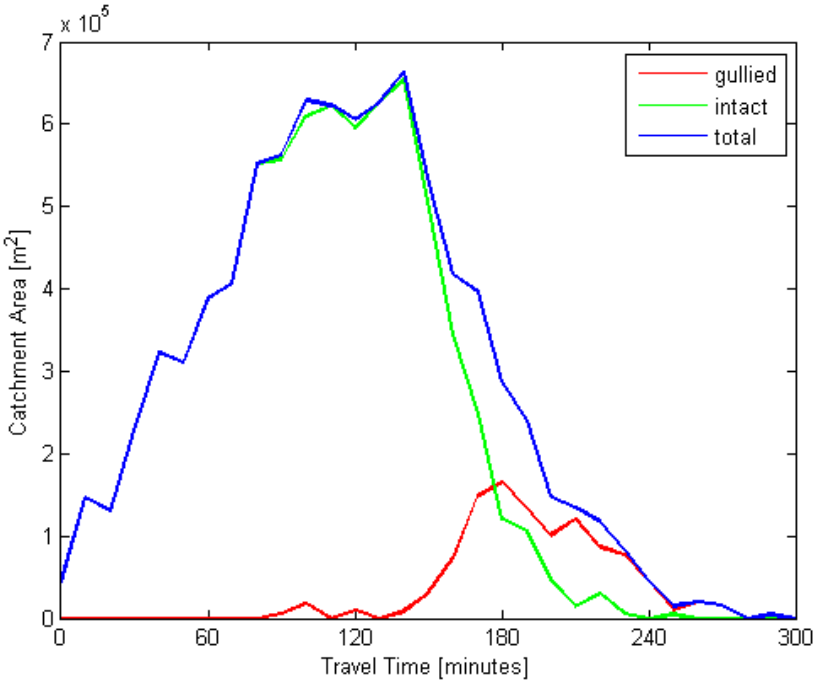

Figure 1.3: Example travel time distributions for gullied and intact HRUs and the entire catchment, the y-axis shows the area of the catchment delivering runoff within the 10 minute period shown on the x-axis. The majority of the catchment is intact, all sub-catchments have travel times less than 3 hours, and gullied catchments have a long modal travel time compared to the intact catchments consistent with the location of gullied sub-catchments in the headwaters.

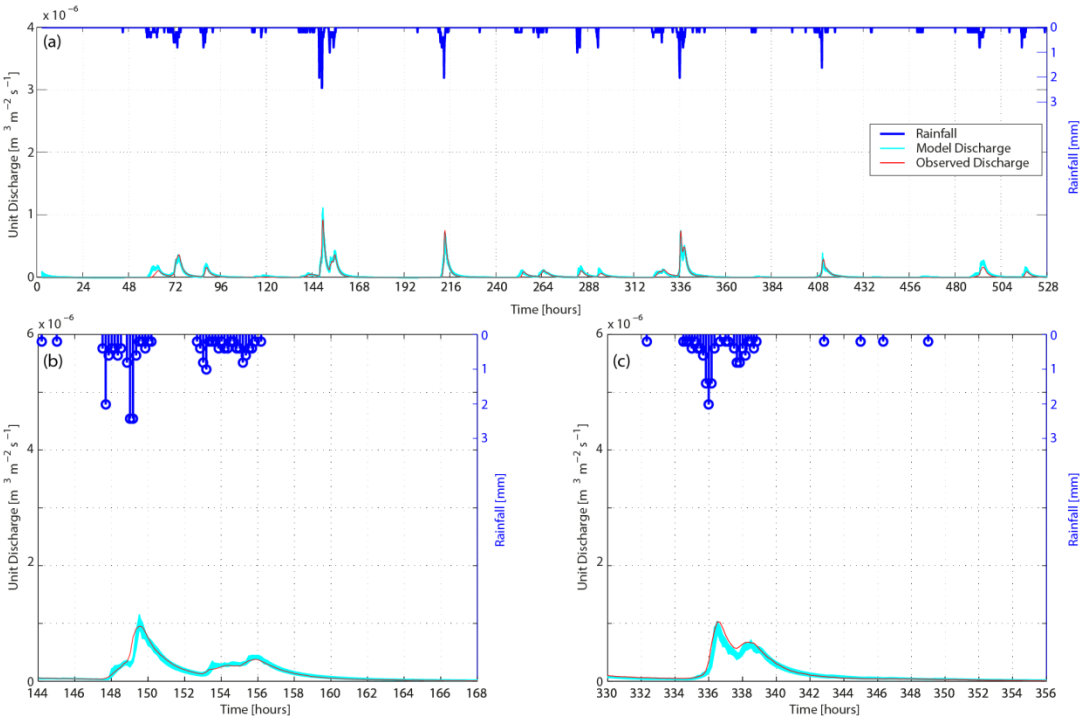

Figure 1.5: Modelled runoff (unit discharge) hydrographs for the intact site for the best 1% of model performances compared with observed hydrographs for: the full study period (a) and the two largest storms (b & C).

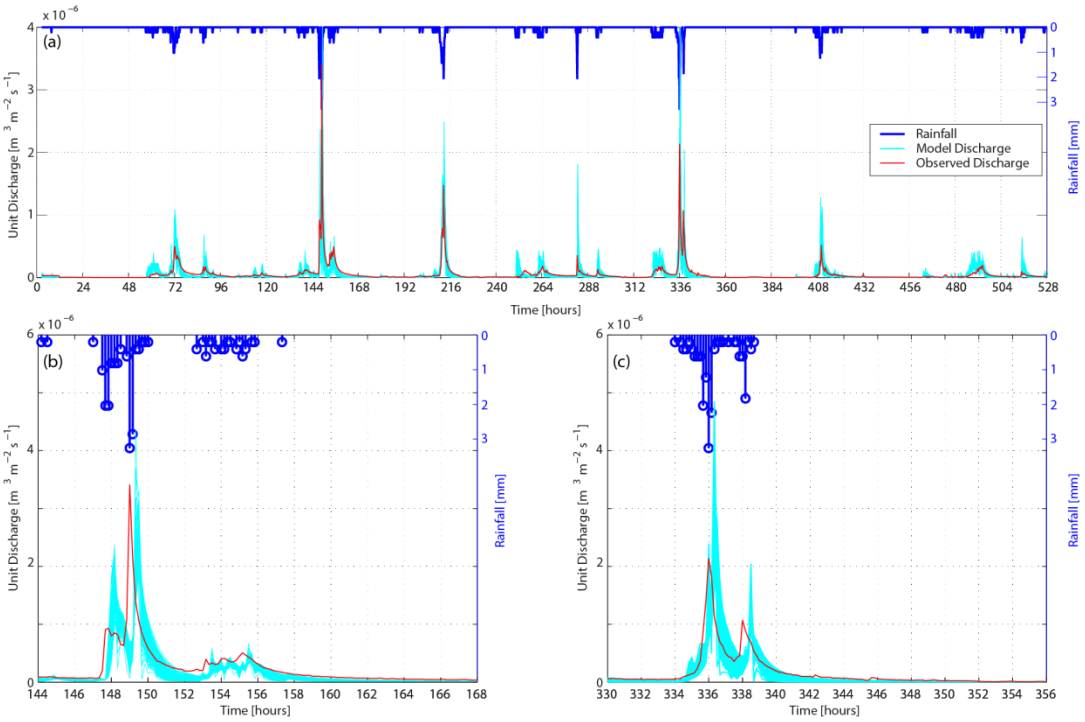

Figure 1.6 Modelled runoff (unit discharge) hydrographs for the gullied site for the best 1% of model performances (using set 2) compared with observed hydrographs for: the full study period (a) and the two largest storms (b & C).

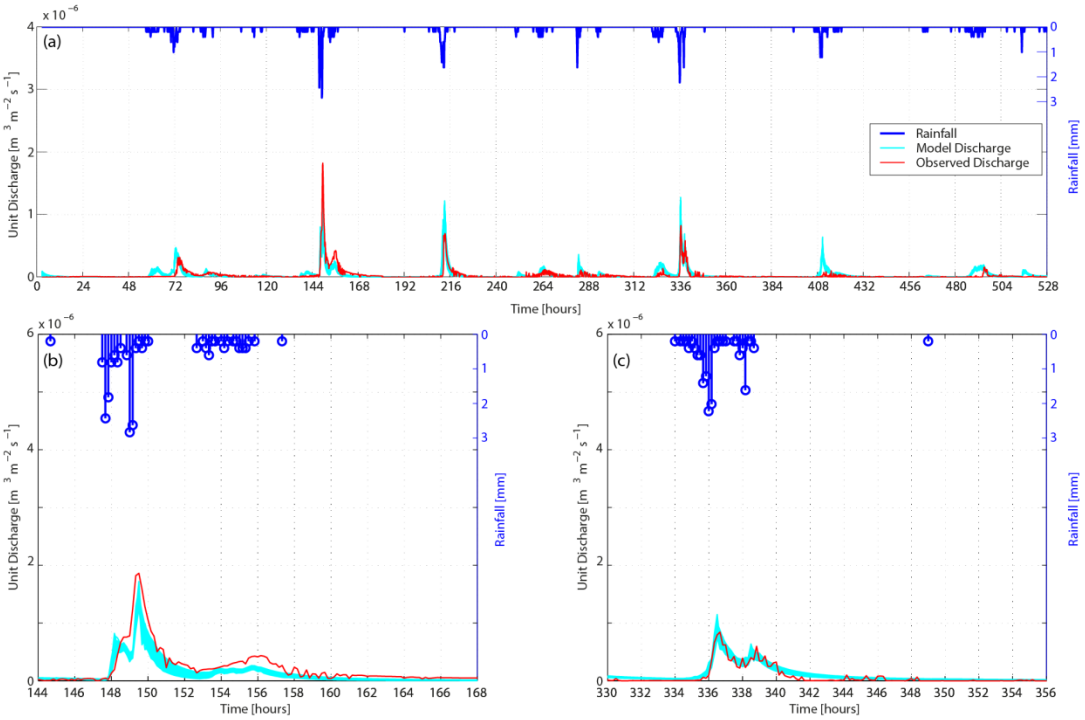

Figure 1.7 Modelled runoff (unit discharge) hydrographs for the re-vegetated and blocked site for the best 1% of model performances (using set 2) compared with observed hydrographs for: the full study period (a) and the two largest storms (b & C).

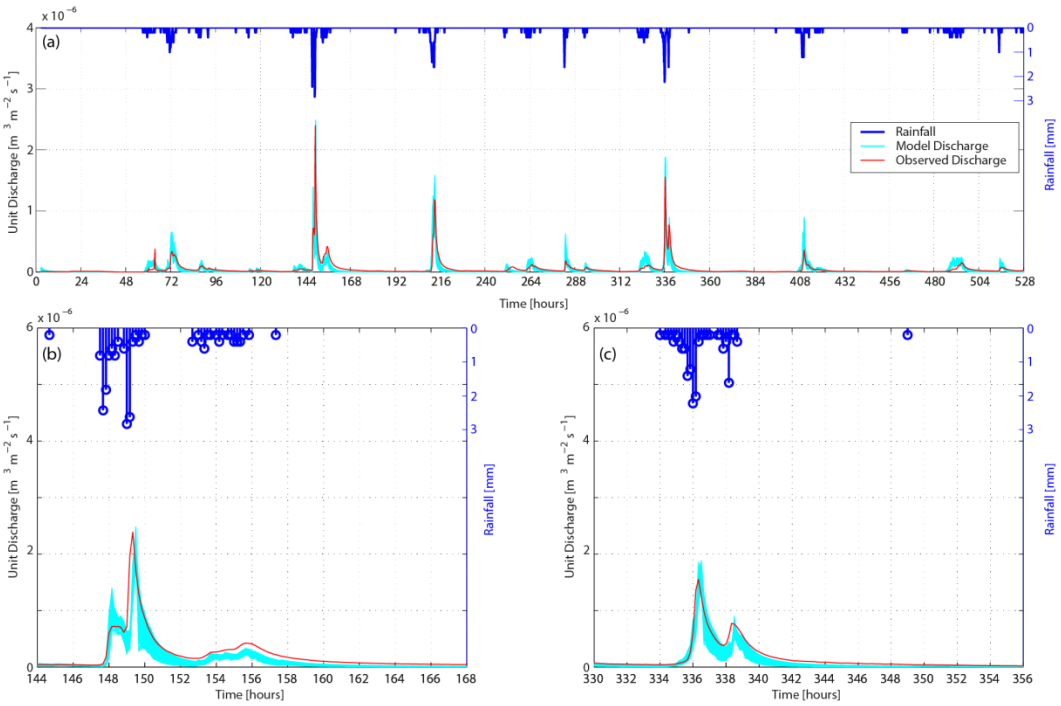

Figure 1.8 Modelled runoff (unit discharge) hydrographs for the re-vegetated site for the best 1% of model performances (using set 2) compared with observed hydrographs for: the full study period (a) and the two largest storms (b & C).

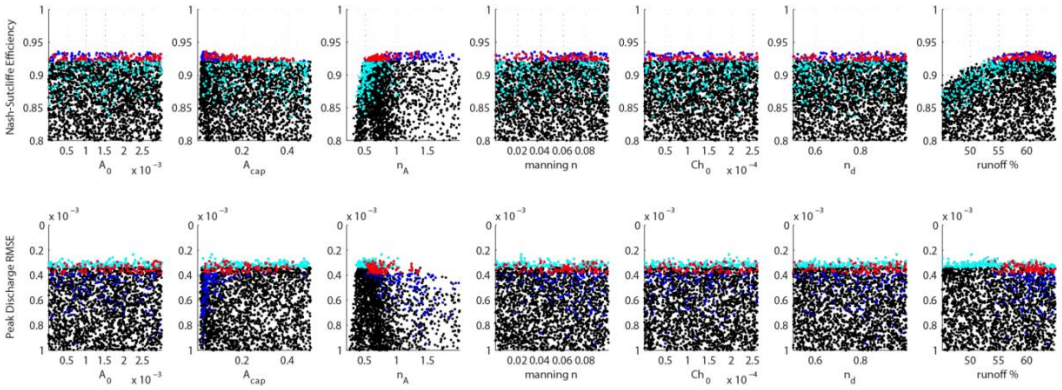

Figure 1.9: MC-based uncertainty analysis plots for the intact micro-catchment.

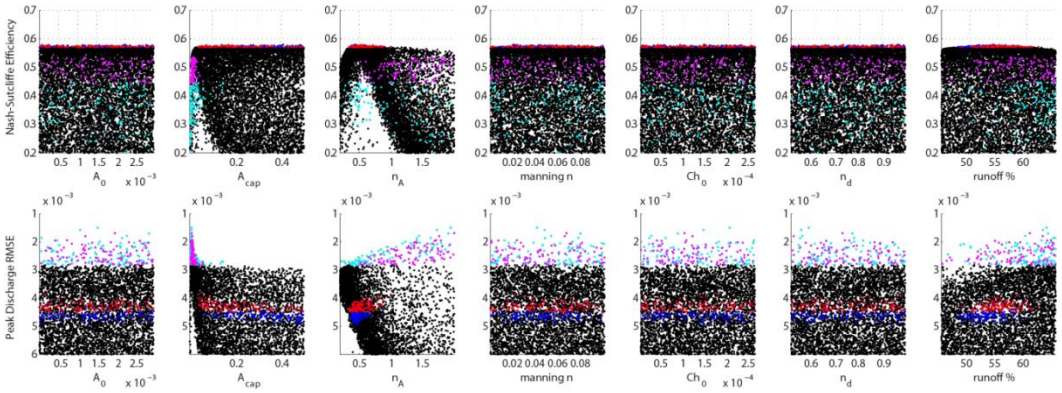

Figure 1.10: MC-based uncertainty analysis plots for the gullied micro-catchment.

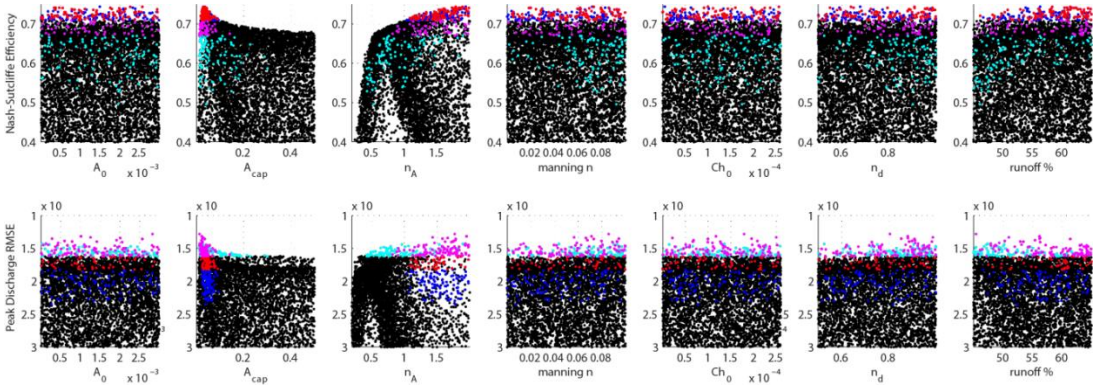

Figure 1.11: MC-based uncertainty analysis plots for the re-vegetated micro-catchment

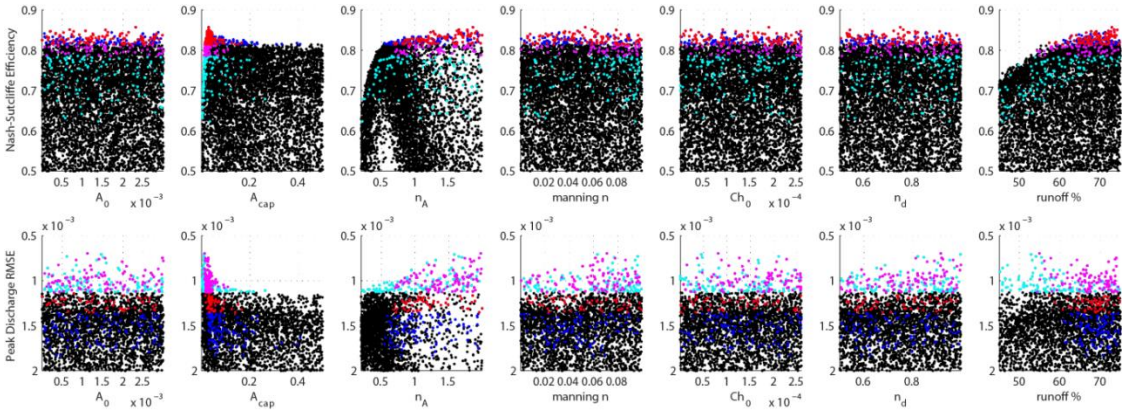

Figure 1.12: MC-based uncertainty analysis plots for re-vegetated and gully blocked micro-catchments.

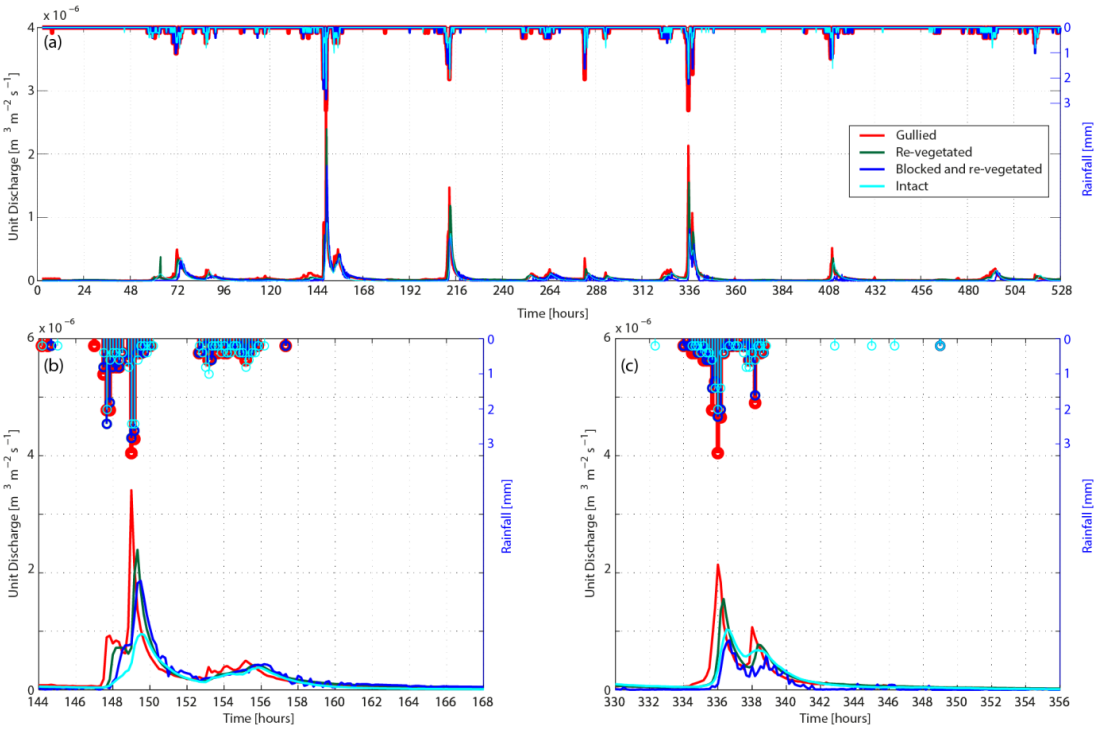

Figure 1.13 Observed runoff (unit discharge) hydrographs for the four study micro-catchments for: the full study period (a) and the two largest storms (b & C).

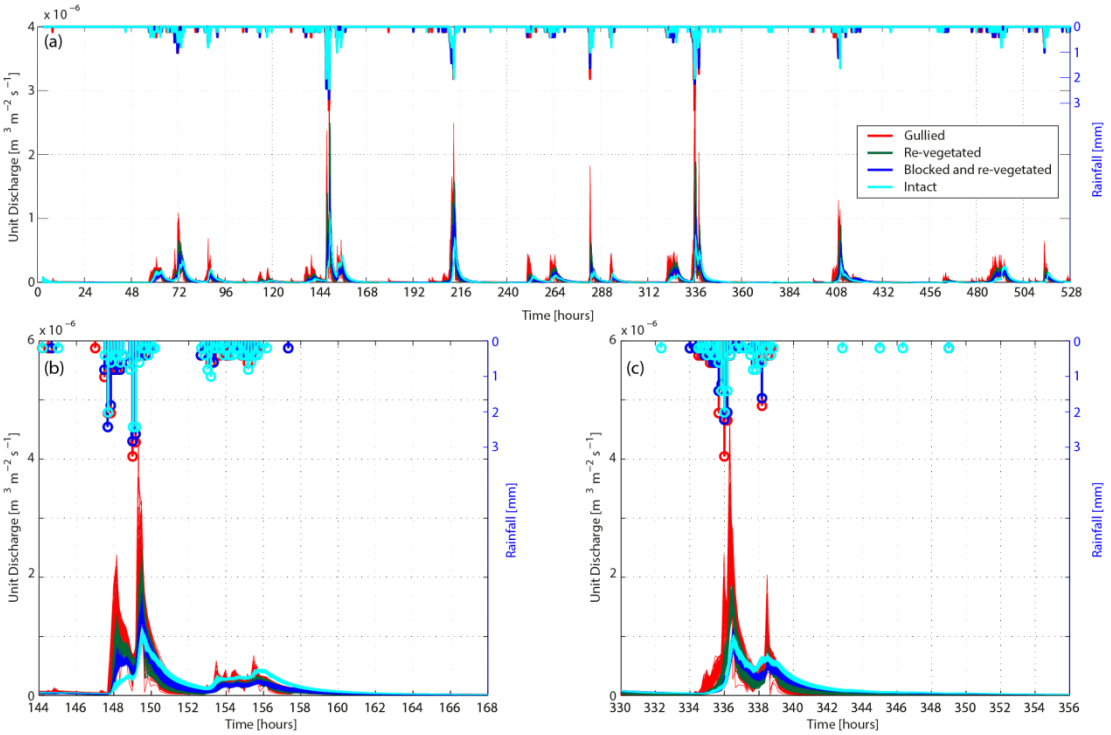

Figure 1.14A Modelled runoff (unit discharge) hydrographs for all sites for the best 1% of model performances (using set 2) compared with observed hydrographs for: the full study period (a) and the two largest storms (b & C). *Note: the catchments' own rainfall is used for each hydrograph*

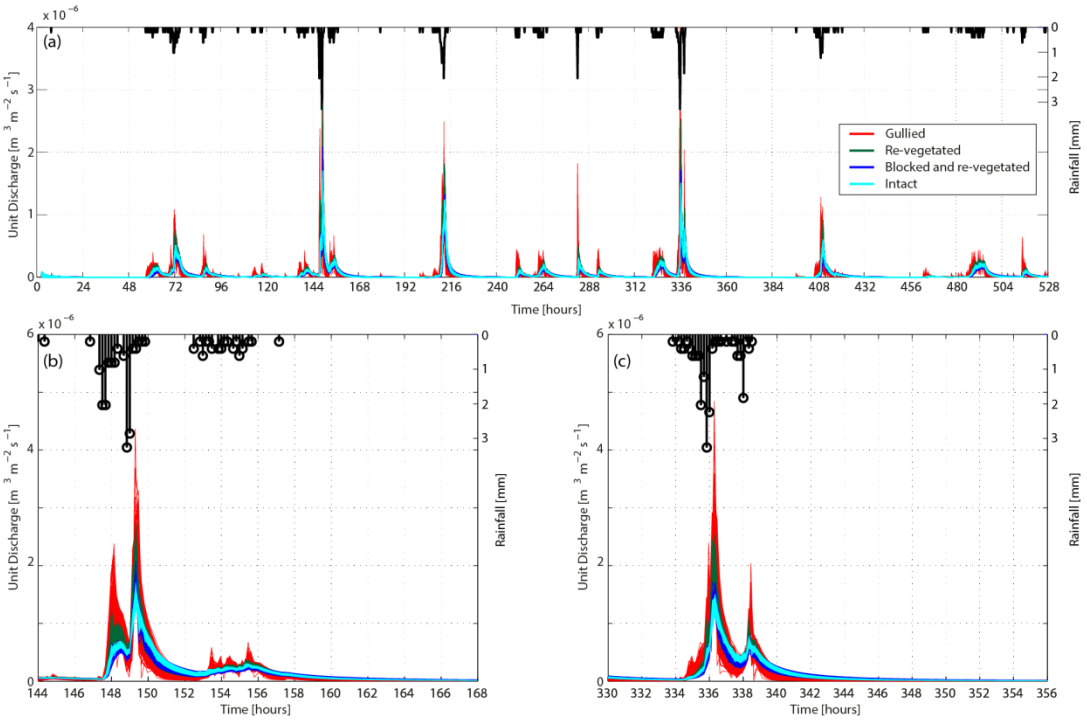

Figure 1.14B Modelled runoff (unit discharge) hydrographs for all sites for the best 1% of model performances (using set 2) and rainfall data from the gullied site: the full study period (a) and the two largest storms (b & c). *Note: the same rainfall is used for each hydrograph*

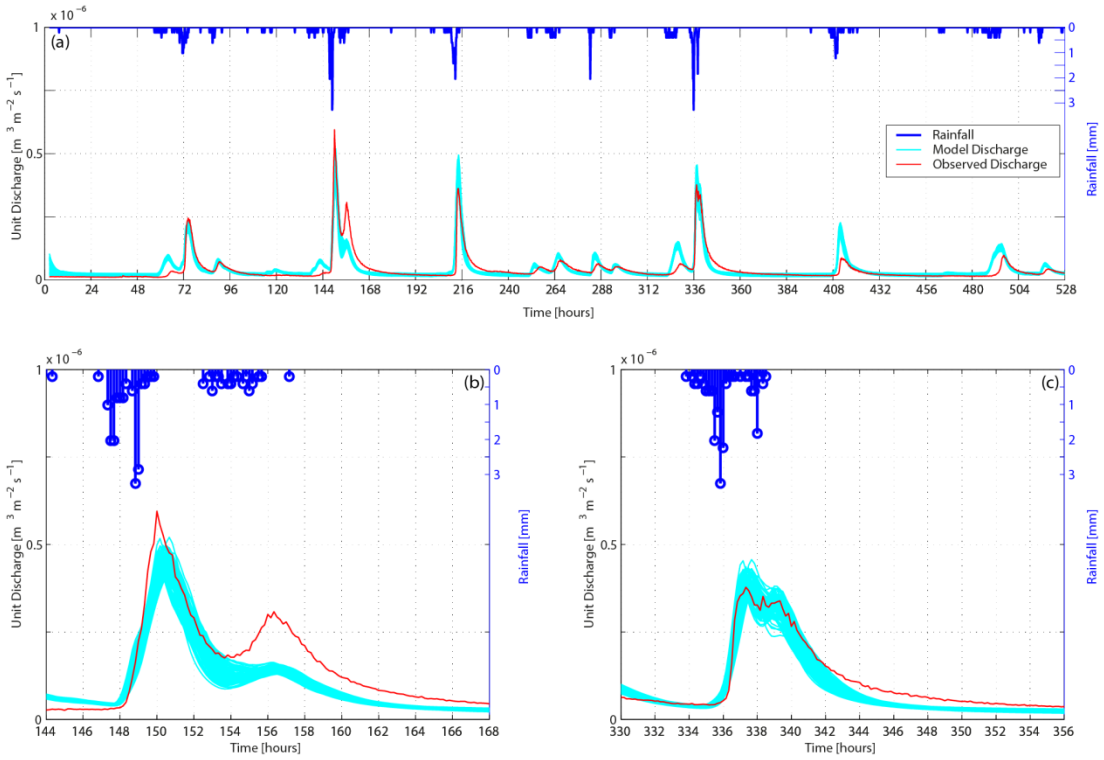

Figure 1.15: Modelled and observed discharge for the upper Ashop catchment. Model results for the best 1% of parameter values using an SDUH model with runoff generated using the lumped models developed and tested at the micro-catchment scale.

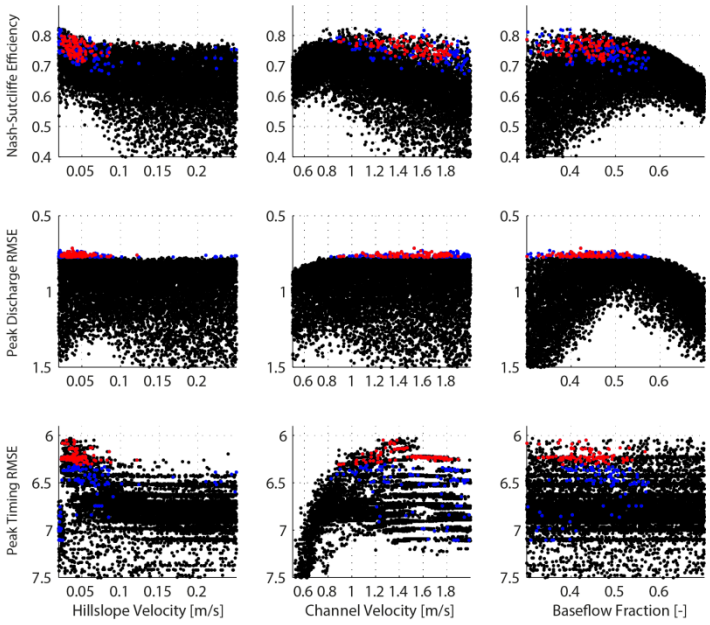

Figure 1.16: MC-based uncertainty analysis plots for the SDUH model (3 parameters) for 3 objective functions: Nash-Sutcliffe efficiency; peak discharge RMSE and peak timing RMSE. Red dots indicate best 1% blue dots represent best 2% from NSE and peak discharge RMSE alone.

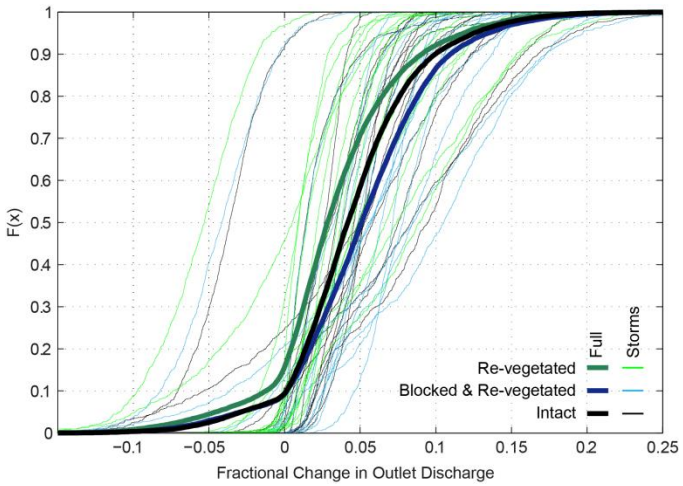

Figure 1.17: Cumulative frequency (F(x)) of fractional change in discharge relative to pre-intervention discharge for 15 largest storms in the study period. Bold lines indicate the relationship for the full data set, thinner lines indicate relationships for individual storms. Note that positive changes reflect reduction in peak discharge.

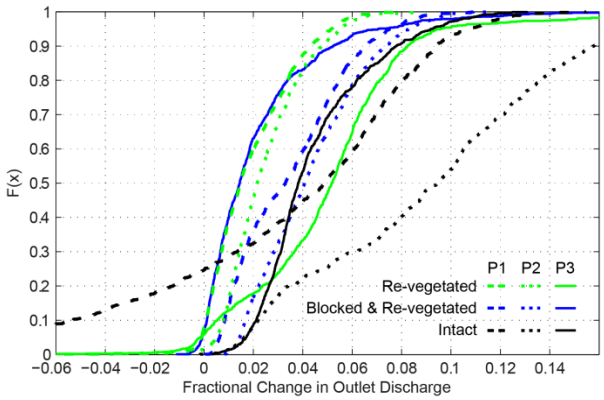

Figure 1.18: Cumulative frequency (F(x)) of fractional change in discharge relative to pre-intervention discharge for 3 largest storms in the study period. Note that positive changes reflect reduction in peak discharge.

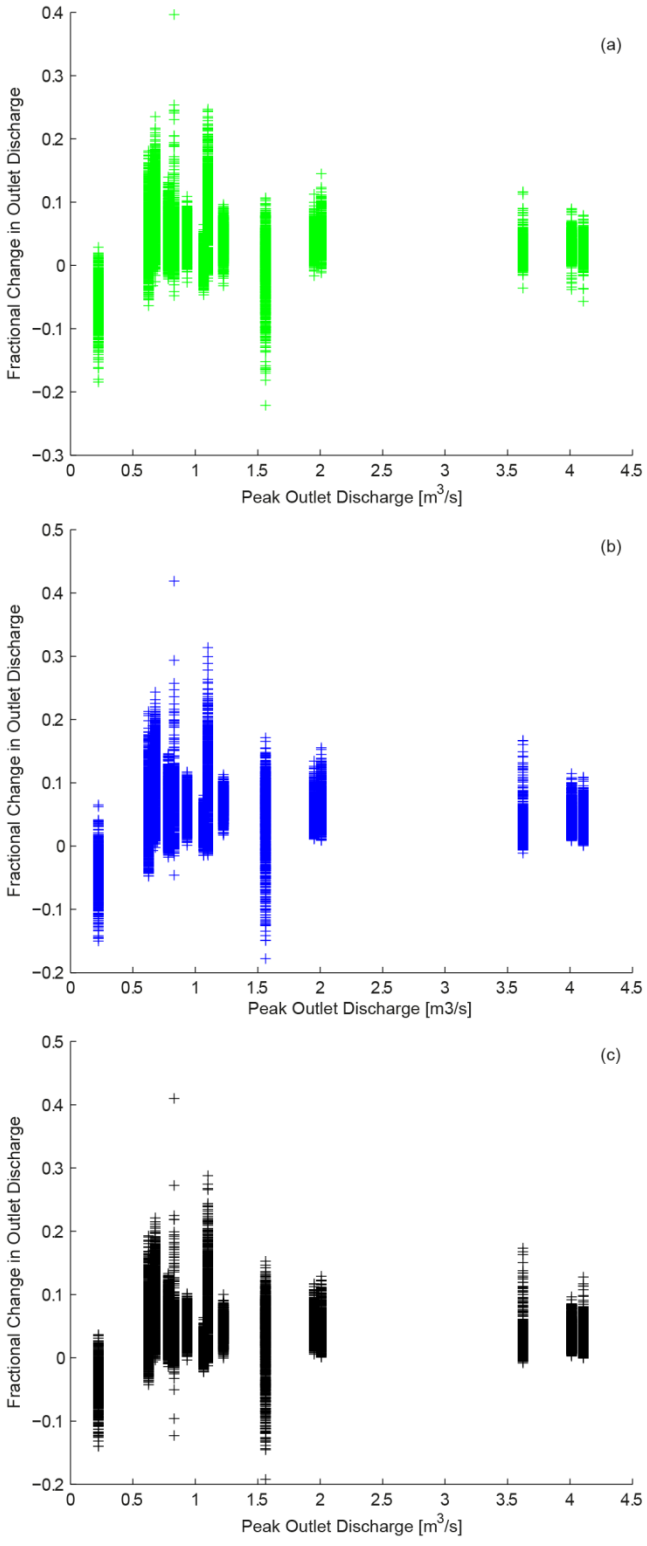

Figure 1.19: Fractional change in outlet discharge against peak outlet discharge for each of the 15 largest storms in the study period and each of the 1000 model simulations. The three panels show results for a) re-vegetation, b) gully blocking and re-vegetation and c) intact scenarios. Note that positive changes reflect reduction in peak discharge.

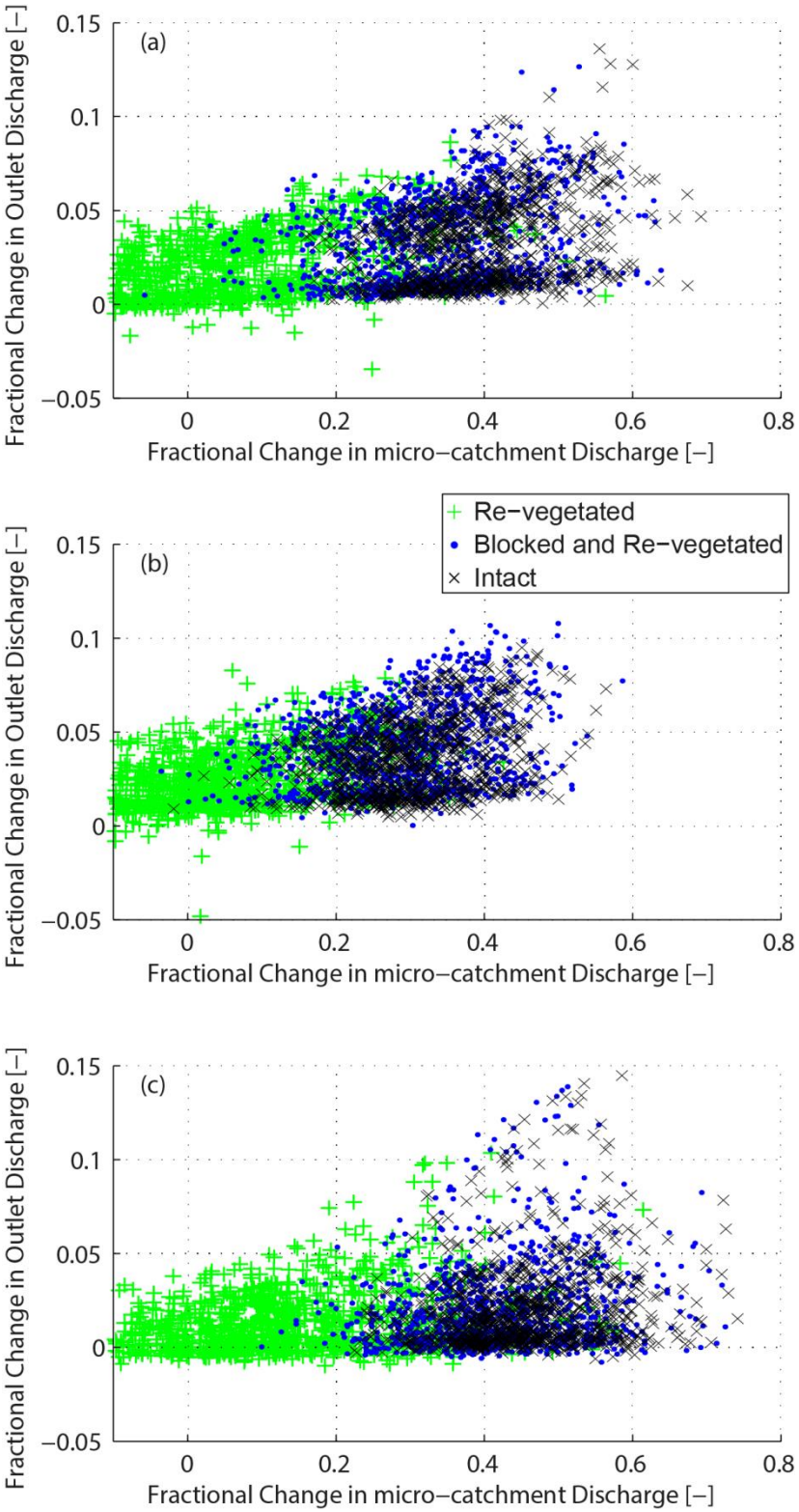

Figure 1.20: Fractional change in outlet discharge with change in micro-catchment discharge based on pairwise comparison for a given parameter set for each of the largest 3 storms in the study period. The three panels show results for a) storm 1, b) storm 2 and c) storm 3. Note that positive changes reflect reduction in peak discharge.

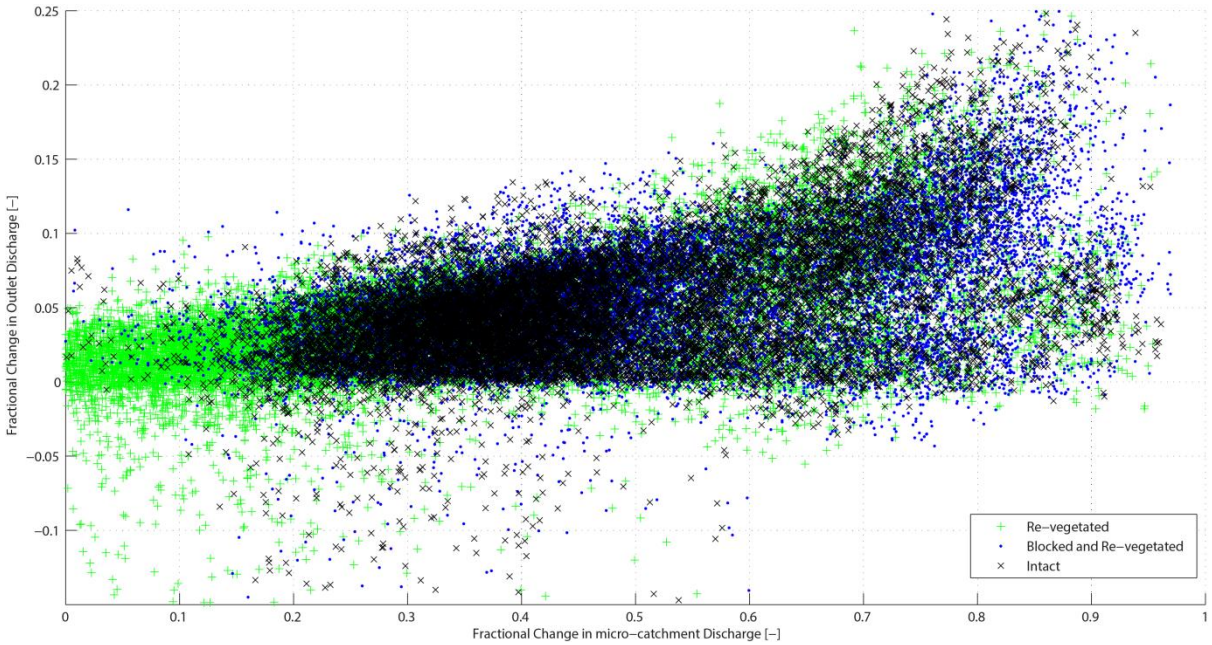

Figure 1.21: Fractional change in outlet discharge with change in micro-catchment discharge based on pairwise comparison for a given parameter set for each of the 15 storms in the study period. Note that positive changes reflect reduction in peak discharge.

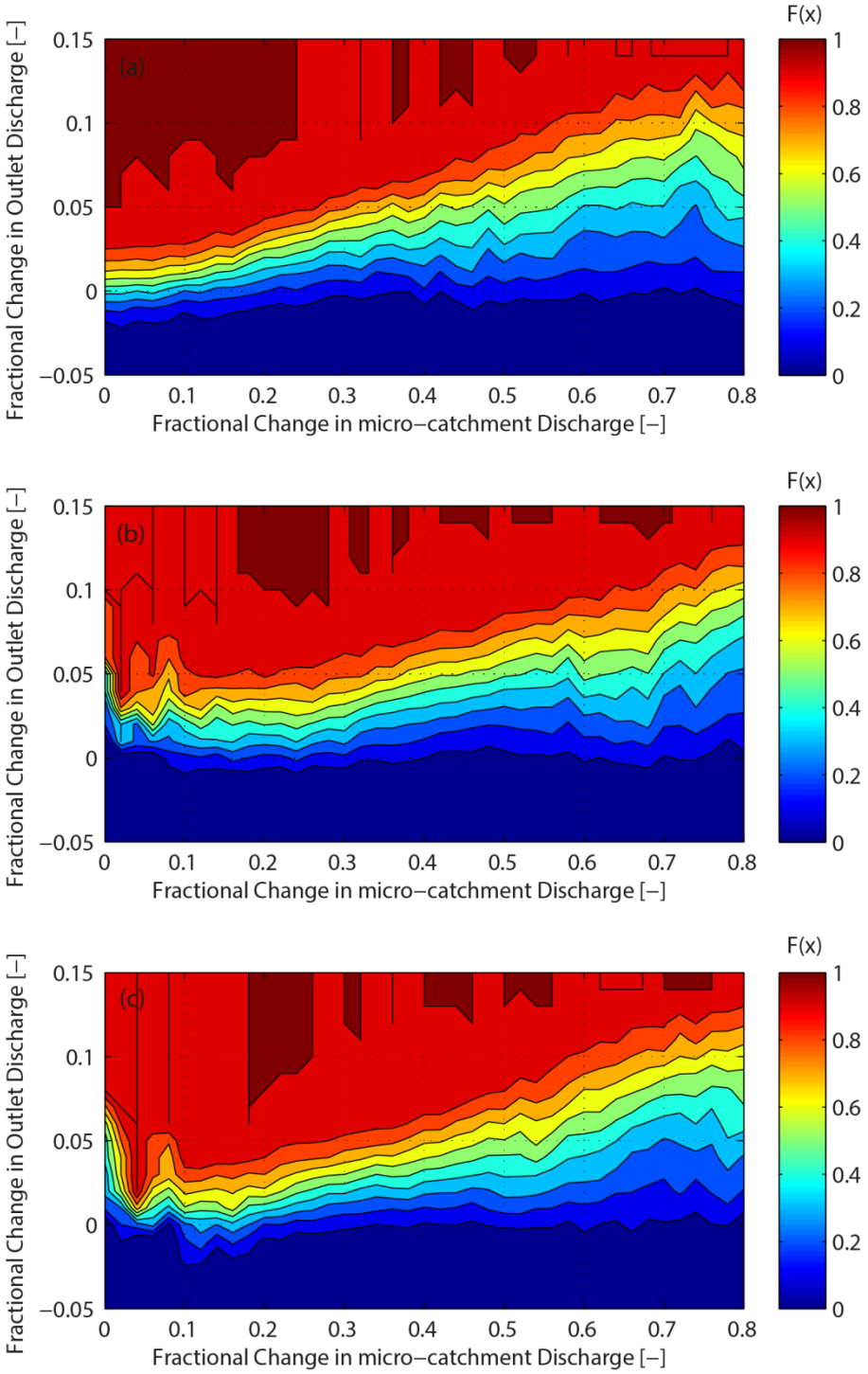

Figure 1.22: cumulative frequency distribution for Fractional change in outlet discharge given change in micro-catchment discharge using pairwise comparison data shown in Figure 1.21 for: a) re-vegetation, b) gully blocking and re-vegetation, and c) the intact scenario. Read these plots as: 'the probability (colour bar) that a fractional change in outlet discharge is less than the y-axis value given that the fractional change in micro-catchment discharge is the x-axis value'. Note that positive changes reflect reduction in peak discharge.

1.6 Tables

Table 1.1: the scenarios tested in this study and the runoff time series assigned to the gullied HRU to generate the gullied component of the discharge.

Scenario	Runoff (R(t)) assigned to gullied HRU
Pre-intervention	Gullied (Firmin)
Re-vegetated gullies	Re-vegetated gullies (Olaf)
Blocked and re-vegetated gullies	Blocked and re-vegetated gullies (Nogson)
Intact	Intact (Penguins)

2 GULLY BLOCK DESIGN

2.1 Background

There is increasing awareness that upland landscape interventions may have a rôle in reducing flood risk to downstream, populated areas (e.g Posthumus *et al.*, 2008; Parrott *et al.*, 2009; Odoni and Lane, 2010 Pattison and Lane, 2012). It is also appreciated that interventions in the uplands which are primarily intended to reduce downstream flooding may have other benefits, for example, in the reduction of gullying, erosion and peat loss from peat moorland. When considering what may be used as intervention measures, land managers will often want to include the possibility of installing small dams or weirs in the streams draining upland sites. The objective in using weirs is to form a temporary water storage zone upstream of each weir that delays passage of runoff during a storm. Provided the weirs are suitably designed and positioned in the stream network, the storage and flow delay effects of weirs should be made evident as attenuation of the flood wave. This attenuation should be quantifiable as: (1) a reduction in peak discharge during an event, and (2) a delay in the timing of the flow peak. This report therefore focuses on aspects of the design and arrangement of small weirs so as to maximise both (1) and (2), and includes an assessment of which types of weir afford the greatest potential usefulness as flow intervention measures.

Although we focus on the behaviour of weirs in this report, this is not meant to imply that weirs alone can prevent or reverse the problems caused by gullying and the presence of extensive areas of bare (un-vegetated) peat. Rather, weirs should be seen as one member of a broader set of interventions, which between them are intended to repair and restore the condition of gullied and bare peat, in turn slowing both erosion and runoff.

With regard to the weirs themselves and what sort of weir to install, the design and installation of weirs has received much attention in the engineering, hydraulic and hydrological sciences, although most research has focused on large rivers (>100 km^2), with little work referring to the use of small weirs in upland catchments. This report therefore deals specifically with the types and sizes of weirs that might be suitable to use in upland peat gullies, at the sub-catchment or micro-catchment scale (respectively <1km^2 and <10ha). The research is carried out by way of a simulation modelling study, but with an eye throughout on how things are likely to be done practically on real peat upland sites.

In the modelling, the main aim is to apply simple mathematical models to make evident the effect of weirs on flow discharges, and hence the attenuation, if any, caused by the weirs. The model boundary conditions have been chosen to represent real conditions in upland peat catchments (e.g. size of the weirs and ponds, spacing between them, the need to avoid downstream scour, etc.). As the effectiveness of weir interventions may differ between one site and another, depending upon site characteristics, the modelling is applied to two sites, used as exemplars of end-member states commonly found in the peat uplands of the Great Britain: Penguins – “P” - an intact peat catchment of 0.5 ha with almost complete vegetation cover; and Firmin – “F” - a gullied catchment of 0.7 ha with extensive bare peat. Both sites are situated in the South Pennines (Figure 2.1), and summary details of each are given in Table 2.1.

2.2 Model description, assumptions and weir designs tested in this study

In this study the gauged discharge hydrograph from each site during a known rainfall event is used as the upstream input in a simple, dynamic (time-stepped) weir model, which in turn calculates an output hydrograph. By comparing the output with the input hydrograph we can quantify by how much a flood wave is attenuated by a weir or series of weirs, whether reducing the peak discharge, delaying the timing of the peak, or both. To assess the impact of multiple weirs, they can be arranged in a cascade, where the output from the first weir becomes the input into the second, thence the second into the third, and so on. This allows the effectiveness of different numbers and designs of weirs to be compared.

Each weir in the model is envisaged as a single, sharp-crested board, or wall, installed across a gully. 'Sharp-crested' weirs in this context are assumed to have a weir board <15 cm thick, so that there is negligible change in the flow depth between the upstream and downstream edges of the weir's brow or crest.

It should be noted also that some of the terms in this report differ from those commonly used in the engineering or hydraulics literature. Engineers use the term weir 'length', commonly defined as the length of the weir crest between the channel banks (crossing the flow direction), and 'width', again commonly defined as the thickness of the weir's wall, measured flow parallel. Our interest here is in both the weirs and the ponds that form behind them, so for consistency the span of a weir across the stream is also termed here its 'width'. Thus the widths of the stream, of the weir pond, the brow of the weir and the crest of the weir are all read and understood to be measured in the same orientation i.e. at right angles to the direction of the flow. 'Length' is then used for the length of the weir ponds and stream reaches. The thickness of the weir board is measured flow parallel and is assumed to be negligible compared with the length of the weir pond, and therefore can be ignored in the weir model calculations. These and other weir model terms are explained and illustrated below, beginning with the basic dimensions in Figures 2.2 and 2.3.

The volume of water stored behind a weir depends upon the length, width and depth of the weir pond. These in turn depend upon the geometry of the stream banks or gully sides and the long profile gradient of the stream or gully. For a weir implemented singly, or as the first in a cascade, the length of the pond, *L*, will increase in the upstream direction as more water is stored behind the weir board (Figure 2.2). The rate of extension (of the pond's length with water depth) will depend on the gradient of the gully upstream of the weir. However, where the pond is confined between two weirs (i.e in a cascade), the pond length is assumed always to be the distance between the weir boards. The full width of the weir is assumed to be that of the brow, *p*, which is the top of the weir board between the gully sides (Figure 2.3).

As a general point, the brow and crest of a weir are always assumed to be perfectly horizontal. Therefore, in the simplest weir design - the full brow weir (Figure 2.3) – there is no slot or notch, so the crest and the brow are in effect the same dimension and the water flows evenly over the brow with a uniform depth (Figure 2.4). Note also that for all of the weirs – whatever their design - there is assumed always to be freeboard between the brow (or crest if there is a slot or notch) and the level of water in the stream or pond downstream (Figure 2.4). In this way, we assume that the weirs are never "drowned", even at high flows.

The example here is a full brow weir. Where a slot or notch is included in the design, the width of the crest of the weir is smaller than the width of the brow. The simplest design is the rectangular slot weir (Figure 2.5). In this design, the width of the slot (w_0) is uniform, from the crest to the brow. The crest is set at a depth, d, below the brow, so that the flow is usually confined within the slot. However, in high flow conditions the slot may be unable to accommodate the full discharge and the excess will flow over the rest of the brow.

As well as the full brow and rectangular slot weirs introduced above, we consider three other designs, the V-notch, inverted V-notch and letter box slot (or more simply, the "letter box"). Regarding the V-notch weir, the main dimensions are shown in Figure 2.6.

This design is different from the others tested in this research, in that there is no crest as such, only the base of the V. The shape of the V is instead determined by the top width (w_{top}) and the depth of the base of the V below the brow (d). These two dimensions therefore govern the notch's angle. In the engineering and hydraulics literature, studies and reports concentrate on the notch angle, and usually limit this to one of three commonly used values, 60º, 90º and 120º. For practical reasons in this report, and keeping in mind always that weirs need to be constructed and installed on site, we think it more helpful to focus on the top width (w_{top}) of the V-notch weir rather than the notch angle.

The inverted V-notch design (Figure 2.7) appears just as it says, simply as an upside down version of the V-notch. It follows that the apex of the inverted V is level with the brow, and the shape of the weir and notch angle are determined by the notch depth, d, and crest width, w_0.

The fifth design considered is the letter box weir (Figure 2.8). This is like a rectangular slot weir but with a closed top, and is thus a slightly more complicated configuration than in the other designs.

The diagram shows how the crest is set below the brow at depth z_1. The letter box itself has a uniform crest width, w_0, and a height from the crest to the top of the box, d. Thus there is freeboard between the brow and the top of the box, z_2. In this research, we assume that such weirs are likely to be constructed using planks, so the freeboard should not be less than the thickness of a slim plank, taken to be 4 cm. Similarly, although the depth of the box, d, could be set very small, for example to perhaps a few millimetres, we consider this to be unrealistic, as it would be both hard to set accurately in the field and likely to be blocked frequently by peat and other debris. We therefore set a practical working minimum value for d of 2 cm. In the simulations, therefore, d is allowed to vary between 2 cm and whatever maximum value can be accommodated within the full board's depth, z_1, but so as always to leave at least 4 cm of freeboard, z_2.

Taken together, the five different weir designs introduced above are thought to be typical of the designs that might practically be installed in the field. The model therefore affords each of these designs to be tested, both singly and in a cascade. As a general point, for all weir designs, so as to take account of the stream gradients on sites P and F, the weir separation is limited to 7 m and pond widths to 3 m. Also the maximum crest depth (d or Z_1 as appropriate) is limited to 20 cm. Before turning to the results from the simulations, however, some explanation is required of the basic model quantities and mathematical relations.

2.2.1 Basic system quantities and mathematical relations in the model

In general in the model, water flows into each weir pond where there is a volume of water stored behind the weir, and in turn, water flows out of the pond over the weir's crest or brow at a rate depending upon the flow conditions. Regarding flow discharge over the crest and brow, basic physics (Bernoulli's equation) shows that the flow rate is primarily determined by the depth of water over the crest (or brow), measured just upstream of the crest and, where practical, also upstream of a position where the water surface starts to exhibit slope curvature in the downstream direction. Depth of the flow is therefore a crucial term in the flow equations, whatever their form, and in the model the most basic relationship is one which allows flow depth over the weir to be derived from pond volume and vice versa.

Beginning with the volume calculation, Figure 2.2 shows that the water surface in the pond, whatever the weir design, has a slight downward slope in the downstream direction, with some slope curvature (the slope getting slightly steeper) as the flow nears the weir crest. At the same time, the gully through which the stream flows and which the pond occupies may be slightly wider at the downstream end, giving the pond a gently tapered appearance in plan view (Figure 2.3). For simplicity here, it is assumed that the water surface gradient is small and has negligible effect on the pond volume calculations, and can be ignored. Similarly, it is assumed that variations in the width of the pond are negligible for the purposes of calculating the pond's storage volume. Each pond is therefore treated as if its width is uniform and the same as that of the brow of the weir (Figures 2.3 to 2.8), as defined above. Similarly, the pond width is assumed to be uniform with depth, *h*, the slope of the valley sides having a negligible effect on the pond volume calculation.

Given these simplifications and assumptions, and assuming we are dealing with a second or subsequent weir in a cascade (in which case the pond's length is fixed by the distance between the weir boards), then it is possible to calculate the flow depth over the crest as follows:

$$V = Lph = Ah \quad \text{(eq. 1)}$$

where *h* is the flow depth relative to the crest (e.g. Figure 2.5), *V* is the volume of water stored in the pond (measure above the crest) and *A* is the area of the pond, given by:

$$A = Lp \quad \text{(eq. 2)}$$

where *L* is the ponded length (Figures 2.2 and 2.3) and *p* is width of both the pond and the weir board (Figures 2.3 to 2.8).

For a first weir, as explained above, the gradient of the stream allows the pond's length to extend upstream as a function of the depth and stream gradient, so the relationship between volume and depth has to take this into account and becomes:

$$V = Lph + \frac{1}{2}\frac{ph^2}{S} \quad \text{(eq. 3)}$$

where *S* is the stream gradient. Throughout the modelling, *S* is assumed to be constant, at 0.03, at both sites.

With the basic relationship between volume and depth explained, we turn to the dynamics of the model and the equations of state.

2.2.2 Model dynamics and equations of state.

The state variable being modelled is the volume of water, from which are derived the flow depth and flow discharge. At any time, therefore, there is a volume of water in each pond and it is assumed that there is also a flow into the pond, Q_{in}, and a flow out of the pond, Q_{out}, giving the general state equation:

$$\frac{\partial V}{\partial t} = Q_{in} - Q_{out} \qquad \text{(eq. 4)}$$

where the term, $\partial V/\partial t$, denotes the rate of change of pond volume, *V*, at any instant of time. For discrete time steps, a volume change is then calculated using:

$$\Delta V\Big|_{t_1}^{t_2} = \Delta t \times \left(Q_{in,1} - Q_{out,1}\right), \qquad \text{(eq. 5)}$$

where $\Delta V\Big|_{t_1}^{t_2}$ is the change in volume during the time step occupying the period from t_1 to t_2 , Δt is the length of the time step (equal to t_2 minus t_1), $Q_{in,1}$ is the input to the weir pond at time t_1, and $Q_{out,1}$ the flow discharge over the weir at the same time . Having calculated the volume change, the volume at the end of the time step is given by:

$$V_{t_2} = V_{t_1} + \Delta V\Big|_{t_2}^{t_1}, \qquad \text{(eq. 6)}$$

where V_{t1} and V_{t2} are the volumes at time t_1 and t_2 respectively. V_{t2} is then used in equations 1 or 3, as appropriate for a first or subsequent weir, to calculate the flow depth at the beginning of the next time step period, t_2 to t_3; likewise V_{t3} is the initialising pond volume in the time step t_3 to t_4 ; and so on, to the end of the simulation. At every time step, the value of Q_{in} is assumed always to be known: if dealing with a first weir, it is simply the observed discharge from the site or some other stipulated input discharge, as required; if dealing with a second or subsequent weir, it is the output discharge from the weir upstream, plus any reach gain or inflow from a tributary as required.

It should be noted from the above that we do not attempt to provide or employ here a set of fully dynamic flow equations, for example based on the St Venant equations, such as would be used in a complete hydraulic model. In view of the small size of the weir ponds, dynamic flow effects are thought likely to be small compared with the results this simpler weir model will generate. The dynamic conception and equations stated above are therefore considered complete enough for the purposes of this research.

A further simplification is to ignore the incoming velocity of the water coming down the stream i.e. the flow discharge over the weir is assumed to be wholly driven by the flow depth at the weir, with

no transfer of momentum from the flows upstream. For the most part, the incoming velocity effect is considered to be small or negligible, since in most situations the momentum of the incoming water is likely to be heavily damped by its mixing with the much larger volume of water in the weir pond.

2.2.3 Basic discharge-depth relationship and choice of the Bazin equation

As the inflow into each weir pond is always known, the main task in the model is to calculate Q_{out} for every time step and for each weir. Although Bernoulli's equation and more detailed physical analyses can provide a sound basis for the form of a weir equation, in practice empirical parameters are necessary in order to calibrate modelled discharges - based on physical principles – with discharges observed in field or experimental studies. In addition, there are different basic weir equations that a researcher or engineer might use, depending upon the setting, expected flow conditions and so on. This means that the empirical parameters themselves are different between one 'basic' equation and another and subsume within them different physical effects. These weir equations are in turn often adapted to apply to different types and sizes of weir, and modified further to take into account different flow conditions e.g. high, super-critical flows versus low, sub-critical flow conditions.

It is not surprising therefore that a review of the hydraulics and engineering literature finds many weir studies and equations, some of the latter more physically complete than others, and some more generally applicable - across weir types, flow conditions, etc. - than others. In this report, we have sought to keep matters as simple as possible and have used the same equation as the basis for all of the weir designs and calculations. The aim by so doing is to make results from the tests directly comparable with each other, without the need to consider any additional factor through using different basic equations for different weir types. The basic equation chosen for use in this study is therefore the one proposed by Bazin (1886). This is considered to be the most appropriate to use to model discharges over small weirs, where flow depths over the crest are typically expected to be < 25 cm, and in many cases < 10 cm.

With regard to the general form of the equation, this is to be found in many standard texts (e.g. Horton, 1906; Nagler, 1918**;** Williams and Hazen, 1933). Rearranging terms and using symbols consistent with those introduced above for the purposes of this research, the equation relates discharge to flow depth by:

$$Q = w\sqrt{2g}\left[1+\frac{0.55\,h^2}{(h+D)^2}\right]\left(b+\frac{c}{h}\right)h^{\frac{3}{2}} \qquad \text{(eq. 7)}$$

where Q is the discharge, w the width of the weir's crest, b an empirical parameter with a value of 0.405, c another empirical parameter with the value 0.00984, h the depth of water over the crest or brow (as already introduced in Figures 2.2, 2.4 and subsequently above), D the freeboard of the brow (or crest, as appropriate) above the surface of the next stream or pond (Figure 2.4) and g the acceleration due to gravity. D is held constant in all of the simulations at 0.2 m, which is considered to approximate the conditions found in the field at the two study sites; a standard value of 9.80665 m s^{-2} is used throughout for g.

Where the depth, *h*, is greater than 5 cm, equation 7 is used as stated to model the relationship between depth and discharge. However, during the development of the model it was found necessary to make a modification to the Bazin equation in order to apply it to flows < 5 cm deep. The modification takes the form:

$$G(h) = \beta_1 h + \beta_2 h^2 + \beta_3^3 \qquad \text{(eq. 8)}$$

where β_1, β_2 and β_3 are parameters with the values 0.516. 1.144 and 9.180 respectively, all found by regression. $G(h)$ then replaces the expression in parentheses in equation 7 and all of the other terms remain the same. This modification is applied equally to each of the weir designs.

Equations 7 and 8 together therefore provide the basis for all of the weir discharge calculations. Before applying these in the model, however, they have to be integrated, applying mathematical calculus, in order to derive the forms applicable to each weir design, and also taking into account the dimensions of the design.

2.2.4 Using the input data, initialising the model and running the simulations

Input data

For flow input, we use the observed flow discharge data from the two upland sites, P and F (Figure 2.1 and Table 2.1, *q.v.*). The methods associated with this data collection are detailed in Section 4.2.1 of Annex 5. Here we use the period between midnights on 1st and 4th October, 2010, which included two storms, the second being an extreme event causing especially high flows at F. The data are plotted below (Figure 2.9):

The plot shows that the two hydrographs are qualitatively similar to each other, each storm being evidenced by two flow peaks in the discharge at the two sites, and the low flow discharges preceding and following each storm having similar values at each site. However, it will be noted that within each storm event the differences between the first and second peak discharges are small in the P data but much larger in the F data, the latter showing a second discharge peak much larger than the first. It is also interesting to note that the rising limb of the hydrograph and the flow peaks at P are slightly delayed compared with the same at F. The differences between the hydrographs are possibly caused in part by differences in how the storms were experienced at the two locations, but are also likely to be strongly influenced by the different physical characteristics of the sites noted above (Figure 2.1 and Table 2.1, *q.v.*).

It should be noted that the input data are provided in 10-minute intervals, making the input somewhat blocky, a facet evident later in the output generated by the model, particularly for the first weir.

Initial volumes and flow depths

To begin each simulation, it is necessary to calculate an initial pond volume and depth for each pond and weir being modelled. To do this, at the first time step the discharge of the weir system is assumed to be in equilibrium with the flow input. A flow depth is calculated at each weir which generates a discharge matching the input, but taking into account the particular weir design and its

dimensions in the simulation. From the flow depth, the water volume stored in each pond is then calculated, using equation 1 or 3 as appropriate.

h never allowed to be negative

In all of the volume and flow calculations, one condition applies throughout, namely that the depth, *h*, is never allowed to be less than zero. The simulations therefore preclude consideration of those situations where a weir pond may have dried out, wholly or partly, before the onset of rain, so that the initial water level is lower than the weir's crest.

Choice of time step, numerical stability and simulation running time

The simulations were all run using a time step of 10 seconds (equation 5). This was chosen as a compromise value, so as to be small enough to ensure numerical stability in most of the calculations but large enough to allow the model to complete many hundreds or thousands of simulations in a reasonable time (minutes or hours, rather than days or weeks). Occasionally a numerical instability would occur such that a pond would fill too much or empty too much, whereat a simple checking procedure would correct the volume change to a realistic and numerically stable value. This is not as formally correct as would be achieved if applying a Runge-Kutta or similar procedure but is considered quite adequate for the purposes of this research. Mass continuity was also maintained throughout the simulations.

Most single weir simulations were completed in 5 to 15 seconds on a standard desktop or laptop computer, working with an 'i3'® or 'i5'® type processor or equivalent. The full brow and rectangular slot weir simulations were the quickest to run and the inverted V-notch the slowest. The weir model itself was written in Matlab™ and run within that program environment on a desktop or laptop; likewise most of the data pre-processing and the subsequent analyses and plotting were conducted in Matlab™.

2.3 Weir model simulations, I: single weir tests

In the single weir simulations the first aim is to see if there are any patterns of attenuation response which emerge and which are common to the different weir types. Comparison of the outputs should also establish whether one weir type is much better at attenuating flows than the others or all of the designs perform broadly as well as each other.

2.3.1 Full brow design (no notch or slot) .

The full brow weir was found to have no attenuating effect at all on the magnitude of the peak discharge, for either event at either site. The weir does cause a slight delay in timing of the flow peaks, however, some 3 minutes for both storm peaks on both sites. It will be noted that these delay times are within the temporal resolution of the input data.

2.3.2 V-notch weir, rectangular slot and inverted V-notch weir designs

The main response metric of interest is the percentage change in the peak discharge, $\Delta Q_{\%}$, which is calculated using:

$$\Delta Q_{\%} = 100\left[\frac{\max(Q_{obs}) - \max(Q_{\mathrm{mod}})}{\max(Q_{obs})}\right] \quad \text{(eq. 9)}$$

where Q_{obs} and Q_{mod} are respectively the observed and modelled discharges for the storm peak and site of interest. It should be noted that the maximum observed and modelled discharge values are used because the aim is to achieve maximum reduction in the peak discharge. Equation 9 is applied in the same manner for both sites and storms, denoted "P1" and "P2" respectively for the first and second storm peaks at site P, and similarly "F1" and "F2" respectively for the first and second storm peaks at site F.

The simulations with the V-notch weir require the values of two dimensions, w_{top} and d (Figure 2.6), to be changed, so the results are plotted as a response surface, Figure 2.10 showing how the percentage attenuation (equation 9) varies with different combinations of w_{top} and d. The example shown is that for P1. It should be noted that the surface plots for the V-notch weir results for P2, F1 and F2 are qualitatively identical in form to Figure 2.10.

Continuing with Figure 2.10, the surface plot for P1 is generated from a cubic spline interpolation through ~1,700 sample points (simulations) in the model parameter space. The response surface reveals a pattern of increasing attenuation with increased depth of the V-notch and narrowing of the top width, tending to an optimum combination of w_{top} for any given d to achieve the maximum attenuation for the depth of the notch. It is striking how steep the increase in attenuation is with depth of the V-notch, so that the deepest notch – which also has the narrowest top width – achieves the greatest attenuation of c. 4.7%. In addition, however, the surface plot shows that if the top width is set just too narrow for the depth of the notch then the attenuation effect is lost completely. Detailed inspection of model output reveals that this is caused by the narrowness of the notch reducing the discharge too greatly, causing the weir pond to be full to overflowing before the peak input discharge is delivered to the system. Without capacity for further storage, the water spills over the brow without restraint and the weir performs no better than the full brow weir reported above.

Table 2.2 summarises the results for both sites and storm peaks, showing that there is a large difference in peak flow reduction difference between F1 and F2, and a small difference between P1 and P2, the later probably reflecting the similar size of the two P storms. For both sites optimised for the first, smaller storm (P1 and F1) provides maximum attenuation of the peak (P1=4.7%, F1=6.2%) but no attenuation for the second, larger storm. However, optimising for the larger storm provides not only attenuation for that peak (P2=4.7%, F2=0.1%) but also attenuation for the smaller storm (P1=3.7%, F1=1.3%). The time delays on the peaks appear to follow the same pattern though this is difficult to see clearly due to the temporal resolution of the input hydrograph (10 minutes).

2.3.3 Rectangular and Inverted V-notch weirs

Turning next to the results generated for the rectangular slot and inverted V-notch designs, in both designs, the width dimensions being changed are the crest width, w_0, rather than the top width (Figures 2.5 and 2.7). Again, the values of notch or slot depth, d, are also changed, so the results are best viewed as surface plots of the system response. As a general point, the relationship between the response, $\Delta Q\%$, and the dimensions w_0 and d, appears to be qualitatively identical to that seen in Figure 2.10 for the V-notch weir. This similarity of form holds for both storm peaks and sites. Thus

for each weir design, there is an optimal width for the depth of the weir, at which the discharge attenuation is greatest for that weir depth. Similarly, the maximum attenuation increases with depth of the slot or notch, and with reducing width, provided the latter is not too narrow, after which, as with the V-notch weir, all attenuating effect is quickly lost. Again, as with the V-notch example, setting w_0 too narrow restrains the discharge from the weir too greatly, so that the weir pond is filled to overflowing before the peak input discharge arrives. Figures 2.11 and 2.12 show the surface plot for F1, for the rectangular slot weir, and F1 for the inverted V-notch weir, these surfaces being generated from respectively 1,200 and 1,500 simulations and interpolating between the points using a monotonic cubic spline. Tables 2.3 and 2.4 summarise the results for these designs for each storm peak and site.

The results show clearly that both the rectangular slot weir and the inverted V-notch weir perform much better than the V-notch design, for both storm peaks and sites (Tables 2.2–2.4). In percentage terms, the reduction in peak flow for the optimised inverted V-notch for F1 is 25.5% compared with 16% for the rectangular slot and 6.2% for the V-notch (Tables 2.2–2.4). Despite these differences, the similarity of form of the attenuation response to variation in slot width and depth across the 3 weir types is striking. The maximum attenuation is achieved by the deepest weir slot or notch in each case, regardless of the design (Figures 2.10–2.12).

Tables 2.2–2.4 also show a clear difference between P1 and 2 and F1 and 2 in percentage terms; this is likely to be due to differences in the physical properties of the two sites as manifested in their input hydrographs. As with the V-notch results, the rectangular slot and inverted V-notch optimisations for the second (larger) storm result in some reduction in peak discharge for the first smaller storm but not vice versa.

2.3.4 Letter box weir

Interpretation of the results for the letter box weir is somewhat different from the other three types (Figure 2.13). It should be noted that we do not show the all of the results generated using this weir design because out of a large number of simulations it can be seen that the most effective attenuation is caused by setting the crest as deep as possible. We therefore only present the results where the crest depth is held at 20 cm below the brow i.e. z_1 = 20 cm (Figure 2.8). The capacity of the letter box is then adjusted by varying the height of the slot, d, above the crest and the crest width, w_0. In the model runs, the slot height is never allowed to exceed 16 cm, thus maintaining a freeboard or at least 4 cm to the brow of the weir; similarly, the minimum letter box height is 2 cm, as previously stated.

Figure 2.13 shows the surface plot for F1, for the letter box weir, generated from 9,000 simulations and interpolating between the points using a monotonic cubic spline. The results show clearly that for storm F1 (Figure 2.13) the greatest attenuation is achieved when slot height is set to the minimum of 2 cm and the crest width to approximately 390 cm. The attenuation achieved is 34%, considerably higher than that of any other weir design at this site (Table 2.5). As with the other weirs however, the optimum combination of width and slot height is very tightly confined to a steeply sloping ridge, and choosing too narrow a box width for its height causes the attenuation effect to be lost completely. Again the detailed model output shows that a slot which is too narrow causes the weir pond to be full to overflowing before the peak input discharge is delivered to the system.

The steep drop off of attenuation performance is well illustrated in Figure 2.14, this time for the P1 storm. Figure 2.7a highlights the steepness of the ridge for slots that are shallower or narrower than optimum. As in Figure 2.13 the parameter surface has a very sharp curving ridge, which rises with increasing width and decreasing slot depth. The curvature in this ridge is further emphasised in Figure 2.14b. Larger slots afford some attenuation while smaller than optimum slots afford none. Figure 2.14b and c show profiles through the response surface and illustrate the sharp drop off for over-small slots, and also the attenuation achieved for slots that are too wide. For example, the optimal width for a letter box of 20 mm is 120 mm and provides a maximum attenuation of 18.5%, but expanding the width of the same slot to 150 mm (although sub optimal, 25% too wide) still provides attenuation of nearly 14%. Similar observations can be made with regard to the slot depth data in Figure 2.14c.

2.3.5 Summary of single weir results

Figure 2.15a shows the reduction in peak discharge downstream of a single weir of each design optimised to each of the four storms. The letter box weir performs best across all four storms followed by the inverted V-notch and rectangular slot weirs. Storm F2 is very large (almost twice the discharge of F1), whereas P1 and P2 are both smaller and more similar to each other. This helps to explain the similarity is performance of the weirs between P1 and P2 but the disparity between F1 and F2.

It is indeed intriguing that F1 performs so well; this is probably because it is a short but very intense storm, whereas in P1 and P2 the rise in the hydrograph is more gradual so that more of the available storage is filled before the peak arrives. If this is the case then weirs attenuate hydrograph peaks reducing their flashiness but this attenuation changes the shape of the hydrograph in a way that is likely to make additional weirs less effective. F2 is both large and flashy but the weir's impact on this storm is generally modest. We suggest that this effect is related to the limited volume of available storage behind the weirs. Further work is required to examine the influence of hydrograph shape on weir effectiveness.

Figure 2.15b shows the delay in the timing of peak discharge downstream of a single weir of each design optimised to each of the four storms. In terms of timing, the letter box weir is either the best or equal best design at all sites. We are limited in the resolution of peak timings because of the time step of the input hydrograph and the stepped nature of the input. It is difficult to draw a direct relationship between discharge attenuation and timing delay but both are important in terms of downstream effects. Notwithstanding this limitation the time delay appears to show a loose inverse relationship with the size of the storm peak discharge.

2.4 Weir model simulations, II: Weir Cascades

Although a peak attenuation of >20% might appear to be satisfactory against a given site management target it is of interest to see whether this can be increased by installing 2 or more weirs of the same design and dimensions in a cascade. As the letter box design is so clearly the best for both sites and both peaks we explore next the attenuation achieved by a cascade of letter box weirs, focusing particularly on storms F1 and F2. In each case the dimensions used are those found to be optimal for a single weir for each storm (i.e. constant slot width and depth throughout the cascade). We also look in more detail at the time delay as the flow peak propagates down the cascade.

Figure 2.16 shows results for F1 and 2 using the weir dimensions optimised for maximum attenuation of the first storm, F1. The greatest attenuation increment (34%) is achieved by the first weir, and attenuation thereafter is achieved in smaller increments for each successive weir reducing from 4 % at weir 2 to 1% by weir 6. Nonetheless an overall attenuation of 46% after 6 weirs is still a marked increase above the 34% achieved by 1 weir alone.

Further optimisation simulations with the model clearly show that the figure of 46% can be improved upon by optimising each weir in the cascade individually for the attenuated flow passed to it by the weir upstream. Generally, for a given box height, the crest width has to be narrowed slightly with each weir downstream, the highest attenuation approaching very nearly 50% after 6 weirs for the F1 storm peak. For practical reasons, and bearing in mind that the model as presently run does not include reach gain between the weirs, we think it is more useful to apply the same box width in all the weirs in the cascade.

As stated above, attenuation is also made evident in time delays of the peak flow compared with the input. Using the letter box weir, six weirs delay the timing of the peak discharge by ~1 hour for the F1 storm. Interestingly, though the first weir introduces 20 minutes of delay - more than twice that of any other of the weirs in the cascade - each subsequent weir introduces a similar additional delay (~8 minutes) in peak flow. Looking at F2, as is to be expected, by optimising for the first peak the slot width is set too narrow to afford any attenuation in the second peak, the F2 discharge being almost double that of F1. Even so, close inspection of the hydrograph shows that the 6 weirs do introduce a modest delay in the peak flow – 8 minutes after 1 weir and 9 minutes after 6 weirs – and that this delayed flow profile continues down much of the recession limb of the hydrograph.

The results above are achieved by optimising for F1, the smaller event. In a practical management setting it is likely that the aim will be to try to constrain the larger events. It is therefore of interest to establish the extent to which optimising for a high flow reduces the efficacy of weirs in attenuating the lower flows. With this in mind, Figure 2.17 shows for F1 and F2 how introducing a weir cascade, optimised for the larger F2 storm, affects the attenuation of the smaller F1 peak.

Referring to Figure 2.17c we observe the same pattern as revealed in the F1 optimised case (Figure 2.16b), namely that the attenuation increases with increasing number of weirs but that the attenuation increments reduce with each additional weir. For storm F2 we see after 6 weirs an attenuation of ~18% and a delay of 20 minutes in the time of the peak.

Turning however to Figure 2.17b we see that even though this weir design has been optimised for the larger F2 flow peak it has still caused an attenuation of ~20% for the F1 storm and a delay of ~22 minutes after 6 weirs. Thus although some efficacy has been lost the first peak has still been reduced by 20%, a figure likely to be acceptable in many management situations.

We deduce from this that multiple, weirs with sub optimal dimensions i.e. where the crest widths are too wide to maximise attenuation of smaller events, may still nevertheless have a very useful attenuation effect on those smaller flow events. The general message appears to be from this that if there is a choice whether to emplace a weir optimised for a larger or smaller flow event at a particular site, by using the dimension for the larger event optimisation, attenuation will be achieved at both event scales.

While the efficacy of individual weirs decreases very rapidly as their slot dimensions expand from their optima, the efficacy of cascades appears to be less sensitive in attenuating the smaller than optimal peak discharges. Thus, when looking at F1 optimised for F1, the first weir achieves 34% attenuation, but none of the further 5 weirs in the cascade increases the attenuation by more than 5 percentage points, and the sixth weir only adds about 1.5 percentage points to the total attenuation. By contrast, when passing the F1 storm flow through a cascade optimised for F2, although the overall attenuation is about half that achieved by passing the F1 storm through the F1 optimised cascade, there is much less of a difference between the additional attenuation contributed by each weir, some 2.8% for weir 1, 4.7% for weir 2, falling to 2% at weir 6. However, larger than optimal peak discharges result in negligible attenuation even for cascades of 6 weirs, this caused by premature filling of the ponds and weir over-topping, in the manner described above. Given the asymmetry in the relationship between efficacy and slot dimensions and the aim of upstream interventions to reduce downstream flood risk, it seems most appropriate that slot dimensions should be designed 'on the safe side' i.e. by selecting dimensions optimised for the largest expected discharge from a given catchment. This reinforces the other points made above in this respect.

Turning again to attenuation of time, although the additional peak discharge attenuation reduces from around the 3rd weir onwards the extension in time delay is about equal for each weir in the F2 optimised case. Thus, for the F1 storm using the F2 optimised dimensions, each weir from the 2nd onwards delays the timing of the flow peak by ~3 minutes. A similar pattern can be seen in the F2 peak, where each weir from the 2nd onwards delays the timing of the peak by ~2 minutes.

2.5 Discussion

2.5.1 Why does slot geometry affect weir attenuating power?

Weir designs differ in their effectiveness because the different designs have different relationships between discharge and change in pond storage. A weir reduces downstream discharge by holding water up in the pond behind it. Given inflow discharge to a pond the water can either remain in storage in the pond or leave as discharge over the weir. Discharge reduction occurs when the amount of water held in storage in the pond increases because more water is being added to the pond than is flowing out of it. However, for any weir the discharge increases with increasing height of water over the crest of the weir. The relationship between the changing outflow discharge with height and the changing available storage with height defines the relationship between storage and discharge (i.e. the volume of water that will be removed from the flow at a given discharge).

Ideally we would simply close a set of flood gates at each weir at or just before the peak flow (to let though only a much lower discharge). However, there are two problems with this: 1) we cannot know when the peak discharge for a given storm will be until it has happened by which time it is too late (imagine standing by a river in a storm and being asked to identify the peak just before it occurred) and 2) we don't have independent control over when or how much to close the gates (we do not have the luxury of that level of control).

However, by modifying the slot shape we are able to alter the relationship between height and outflow discharge from the weir and therefore to control the relationship between discharge and the volume of water held up in storage. This enables us to design weirs where water height (and

therefore storage) changes as little as possible with increasing discharge at low discharges but where height (and therefore storage) changes increasingly rapidly with increasing discharge.

For the V-notch weir (Figure 2.18) the relationship between discharge and height is non-linear with height increasing most rapidly at lower discharges then more slowly for higher discharges. This is the opposite behaviour to that which we are aiming for. While the increase in height does translate to increased storage most of the storage is used up at low flows with little available storage for high flows. The relationship for the rectangular slot weir is similar but with reduced curvature, indicating that less storage is used at low flows and more is available at higher flows. For the inverted V-notch height (and therefore storage) increases almost linearly with increasing discharge (Figure 2.18), leaving more storage available for high flows. The letter box slot has the slowest increase in height with discharge at low flows then increases more rapidly but still linearly with height once the slot becomes fully submerged. Ultimately it is the slope of the storage discharge relationship at high flows that defines the effectiveness of the weir, the steeper the slope the better. The results in Figure 2.18 are for each design optimised to the F1 storm. As a result each has been designed to fill but not overtop at the peak discharge. The upper break of slope in each curve represents the height at which overtopping occurs and the discharge to which the design has been optimised. This discharge is largest for the least effective weir (V-notch) and smallest for the most effective weir (letter box) since though they all have the same input they each have different output peak discharges. Attenuation through pond storage reduces the peak discharge over the weir. This has important implications for design since it means that a weir will handle input discharges in excess of the design discharge without overtopping. As a result, building slots to accommodate the design discharge is conservative approach. A key next step from this research is the identification of appropriate design discharges: i.e. how do we identify them and which design discharge should we be most concerned about (1:10, 1:25, 1:100 year event)? This might vary from site to site.

2.5.2 Weir Design

In order to implement letter box slot weirs a series of decisions need to be made on a weir by weir basis about the depth and width of the slot. Since the effectiveness of weirs depends on their slot dimensions and storm characteristics we provide some initial suggestions on rules of thumb for slot dimensions based on our simulation results. Design discharges for a weir of any given dimensions can be calculated from the following weir equation:

$$w = \frac{Q}{\sqrt{2g}\left\{\left(1+0.55\left(\frac{z_1}{z_1+D}\right)^2\right)\left(b{z_1}^{3/2}+c{z_1}^{1/2}\right)-\left(1+0.55\left(\frac{z_2}{z_1+D}\right)^2\right)\left(b{z_2}^{3/2}+c{z_2}^{1/2}\right)\right\}} \quad \text{eq. 10}$$

Where: w = width of slot (m), g= acceleration due to gravity (m/s^2); d=depth of slot (m), z_1 = height of board above base of letter box slot (m), z_2 = height of board above top of letter box slot (m) i.e. $z_2=z_1-d$, D = drop from base of letter box slot to pond downstream of weir (m), Q = design peak discharge (m^3/s), b = 0.405; c =0.00984 (both Bazin's coefficients). This equation can be used to calculate appropriate dimensions for any letterbox weir given a design discharge. However, for ease we have evaluated this model for a set of common cases to provide the following simpler equation for slot width:

$w = kQ$ eq. 11

Where: k = a coefficient the values for which are found in Table 2.6; *Q* = design peak discharge (m^3/s).

For example, to install a suitable weir at the outlet of the F catchment (Area = 7,000 m^2), we could choose a slot height of 0.020 m and a depth of 0.2 m then find the slot width from eq. 11 and Table 2.6 as W = 31.4 Q. Taking the design discharge as twice the largest peak unit discharge at any of the study micro-catchments over the study period (i.e. $1x10^{-6}$ m/s) multiplied by catchment area the estimated design discharge would be 0.07 m^3/s. From eq. 11 this gives slot width= 31.4 x 0.07 = 2.17 m.

Note that we have picked an arbitrary discharge for illustration here. Establishing the design discharge for these systems is a non-trivial exercise and should be undertaken as a priority before implementing modifications to weir design. A first step in this direction would involve examining flow duration curves for longer discharge records and tying these together with events from the micro-catchment record to estimate probable maximum storm discharge.

It should be borne in mind that the P and F sites are not large, each being of less than 1 ha, so this limits the possible number of weirs that could be installed in a cascade to ~6 weirs. Considerations of channel gradients and separation of the streams and tributaries also limit how the weirs are separated and what maximum size (storage volume) can be formed for each weir pond. Given the branching nature of gully systems many weirs might be emplaced at a site but these should be emplaced with consideration for the upstream catchment area and therefore design discharge. The size and spacing of weirs is currently designed so that ponds extend back to the next upstream weir under low flow conditions to avoid scour downstream. Our suggested modifications would not alter this spacing consideration but would lead to deeper ponds during high flow events.

We have limited weir separation to 7 m (6 weirs spaced every 7 m along 42 m of channel with top width of weirs 3 m wide, with a slot cut at 0.2 m from the top of the board). This imposes a limit on maximum storage volume in a weir pond. However, pond storage potential is clearly the major contributor to attenuation, so larger (longer) ponds will increase the efficacy of a given weir. Such changes in pond dimensions affect all weir designs to the same degree.

Weir design will likely also be constrained by a series of practical considerations. If the slot is too deep: the pressure of the ponded water may damage the weir board; the jet of water flowing out over the crest could be erosive for peat downstream of the weir or introduce velocity to downstream pond slightly reducing attenuation. If the width or depth of the slot is too small it may become blocked by material that is being transported by flow in the gully.

2.5.3 Further work

Our findings apply to both study sites and both storm peaks, we are confident that the letter box design will be most effective across the full range of discharge conditions. We are less confident about the absolute reduction in peak discharge that will result from a given weir since this is clearly a function of both weir / pond characteristics and hydrograph characteristics. More research is required to unpick the influence of these factors on weir efficacy.

Importantly, this is a mathematical study and the results need to be tested in the field. Such testing could involve monitoring ponds behind weirs before and after modification of the weir design.

2.6 Key results: Gully block design

1. Gully block design can considerably improve efficacy of blocks in both reducing peak discharge and slowing the arrival time of the peak flow.

2. Weir designs in order of efficacy from least effective to most effective are: full brow (almost not effect at all), V-notch, rectangular slot, inverted V-notch, letter box slot.

3. Within a given design the deeper the crest of the slot can be the more effective the weir will have

4. The smaller the slot (the narrower the crest, for a given slot depth), the more effective a weir will be up to an optimum, beyond which the weir overtops and all attenuation is lost. Weirs should therefore be optimised for the largest expected storm (design discharge).

5. Building slots to accommodate the design discharge is conservative: attenuation through pond storage will reduce the peak discharge over the weir, so that a weir will handle input discharges in excess of the design discharge without overtopping.

6. Design widths for letter box slot weirs cut at 0.2 m depth with slot heights of 20 mm scale with discharge as W = c. 31 Q.

7. Cascades of weirs increase attenuation (i.e. 2 weirs do more than 1) but the 1st weir often reduces peak discharge considerably more than each additional weir. The same is true of time delays to peak discharge.

8. Cascades of weirs are more likely to perform well over a range of discharges than individual weirs.

2.7 Figures

a. Study site location map and inset

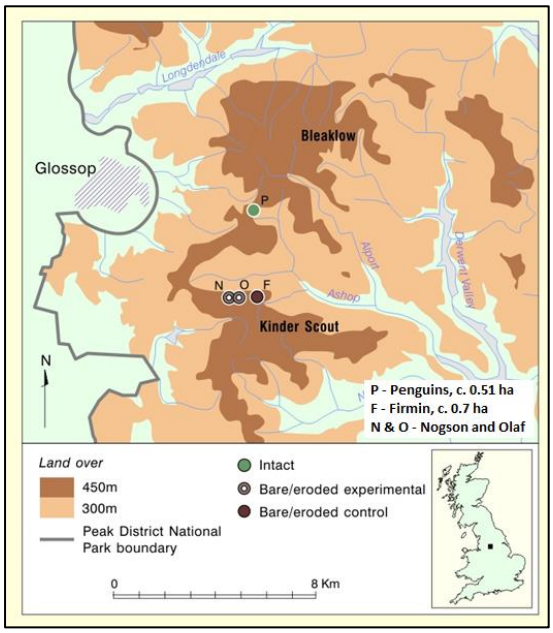

b. Penguins, viewed by the outlet to the site

c. Firmin, showing gullying and bare peat

d. (i) Penguins elevation data, 2m spatial resolution, and
(ii) main flow paths inferred from the topography

(i) Elevations (ii) Main flow paths

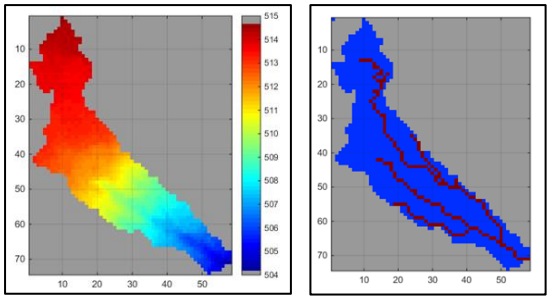

e. (i) Firmin elevation data, 2m spatial resolution, and (ii) main channels and flow paths inferred from the topography

(i) Elevations

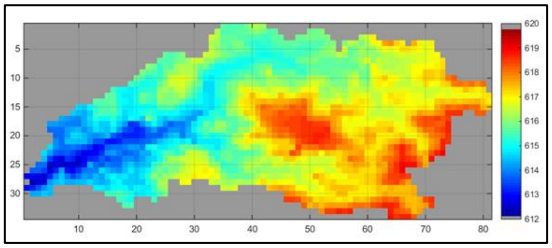

(ii) Main flow paths and channels

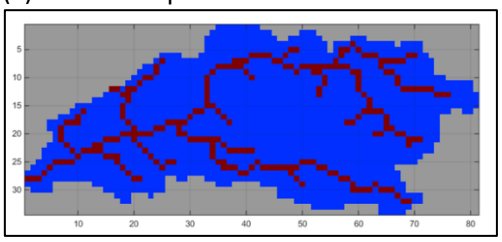

Figure 2.1: (a) location map of the study sites (MFF); (b) and (c), photos taken of the sites; (d) and (e), DEM's of the sites, together with the main flow path or channel network for each site inferred from the topography.

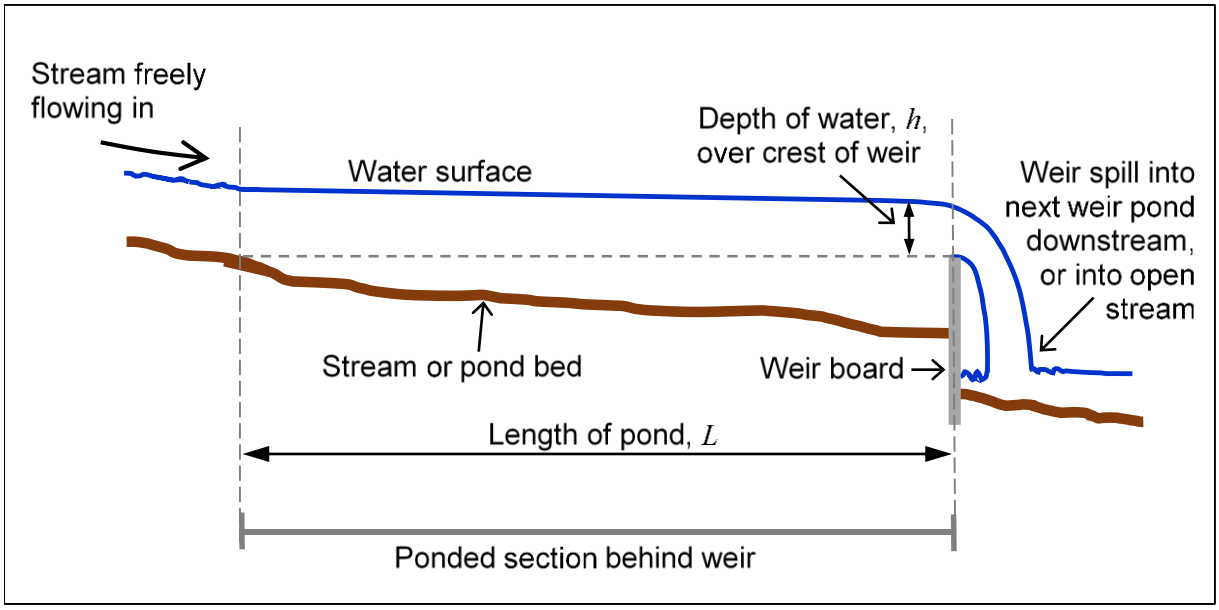

Figure 2.2: diagram of a single weir and pond shown in long profile (side elevation view) and illustrating the main dimensions and relationships used in the weir model.

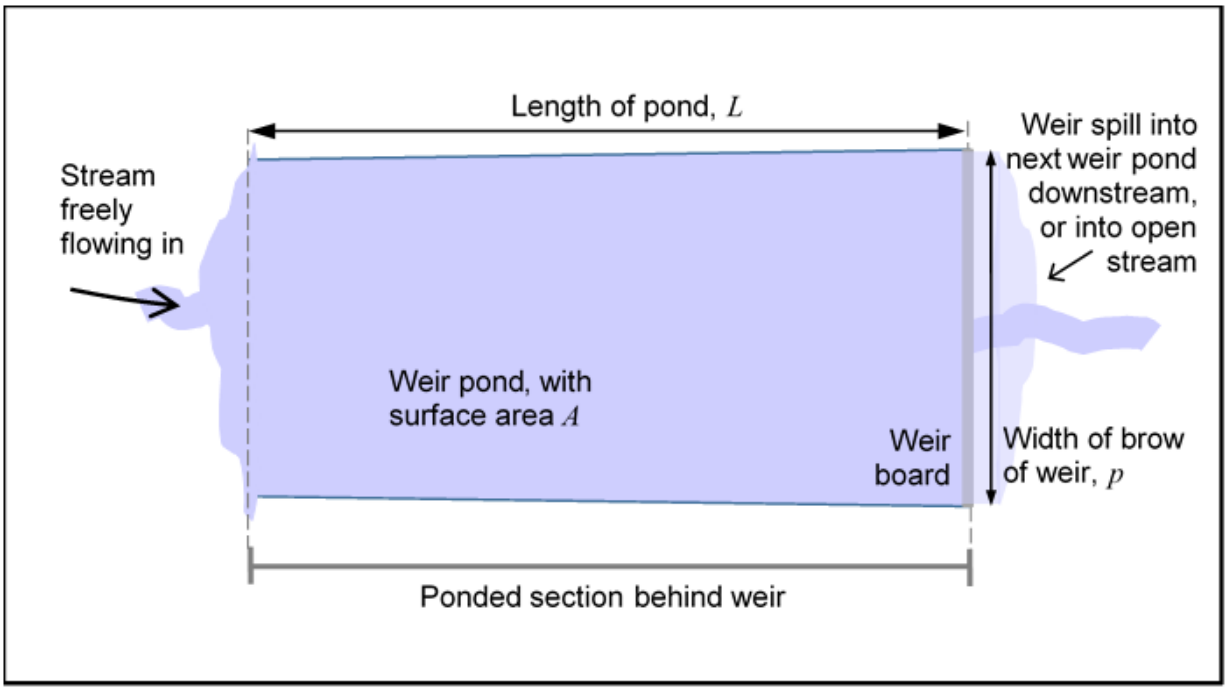

Figure 2.3: diagram of a single weir and pond shown in plan view and illustrating the main dimensions and relationships used in the weir model. The example weir design shown here is of a full brow weir. (See text)

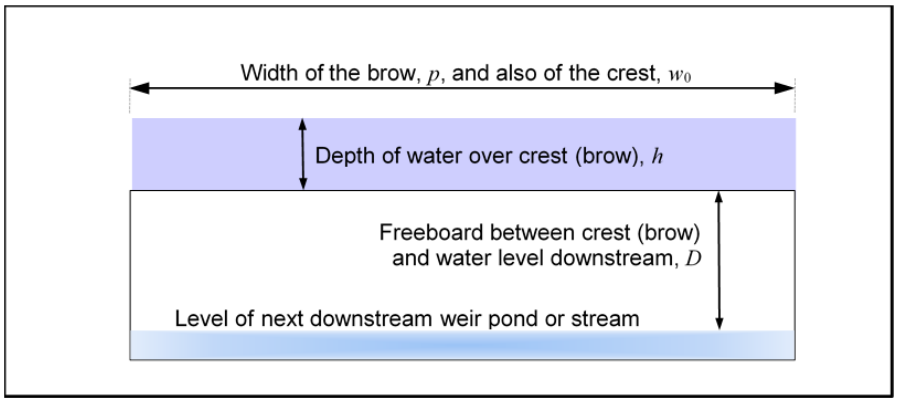

Figure 2.4: diagram of a full brow weir, end elevation view, illustrating the main dimensions and relationships used in the weir model. (See text)

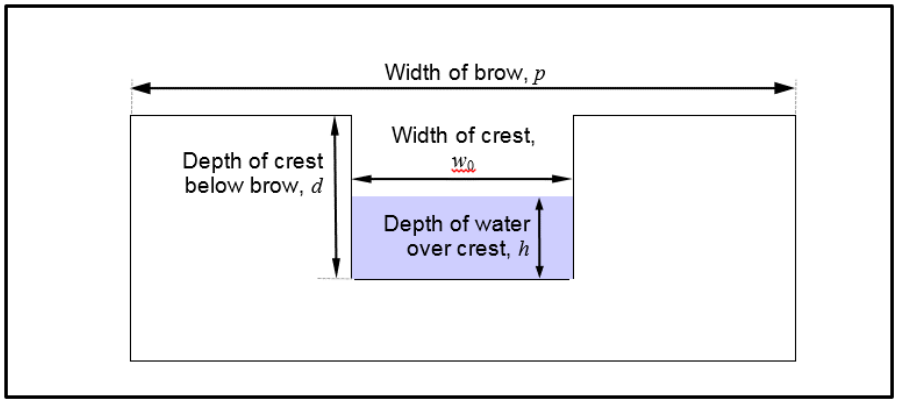

Figure 2.5: diagram of a rectangular slot weir, end elevation view, illustrating the main dimensions and relationships used in the weir model for a weir incorporating such a slot or notch. (See text)

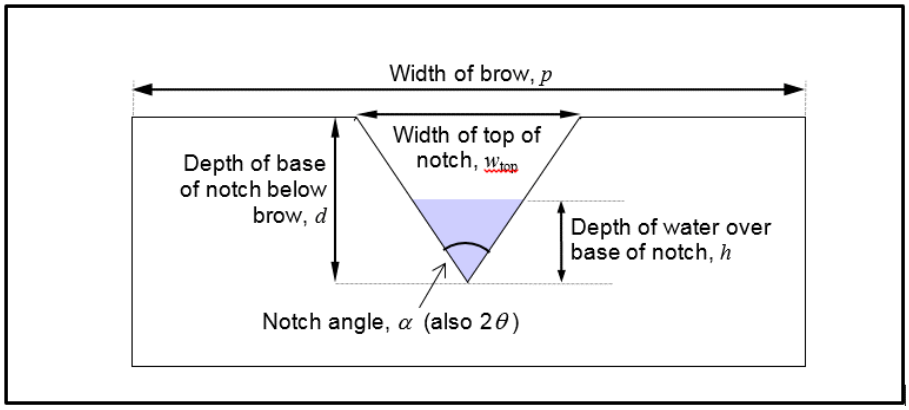

Figure 2.6: diagram of a V-notch weir, end elevation view, illustrating the main dimensions and relationships used in the weir model for a weir incorporating such a slot or notch. Note that this type of weir does not have a horizontal crest, and how the notch angle is determined by the top width and notch depth. (See text)

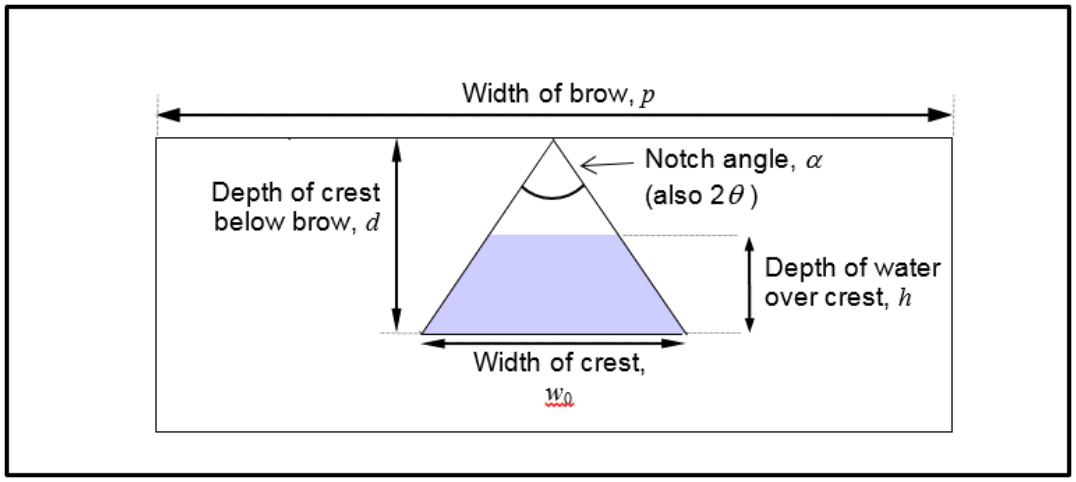

Figure 2.7: diagram of an inverted, V-notch weir, end elevation view, illustrating the main dimensions and relationships used in the weir model for a weir incorporating such a notch. By contrast with the V-notch weir (Figure 2.6), this weir design does include a horizontal crest. Note also that the apex of the notch is level with the brow. (See text)

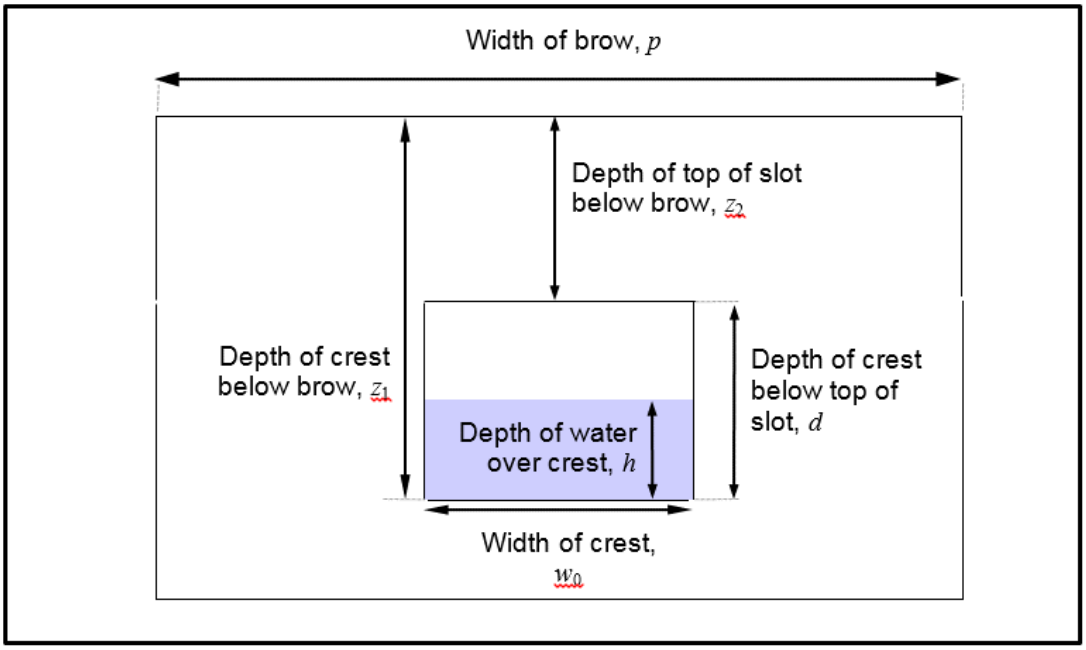

Figure 2.8: diagram of a letter box weir, end elevation view, illustrating the main dimensions and relationships used in the weir model for a weir incorporating such a slot. As with the rectangular slot and inverted V-notch designs (Figures 5 & 7), this weir design includes a horizontal crest. However, the top of the box is set below the brow, so the depth of the box, *d*, is always less than the height of the weir board. (See text)

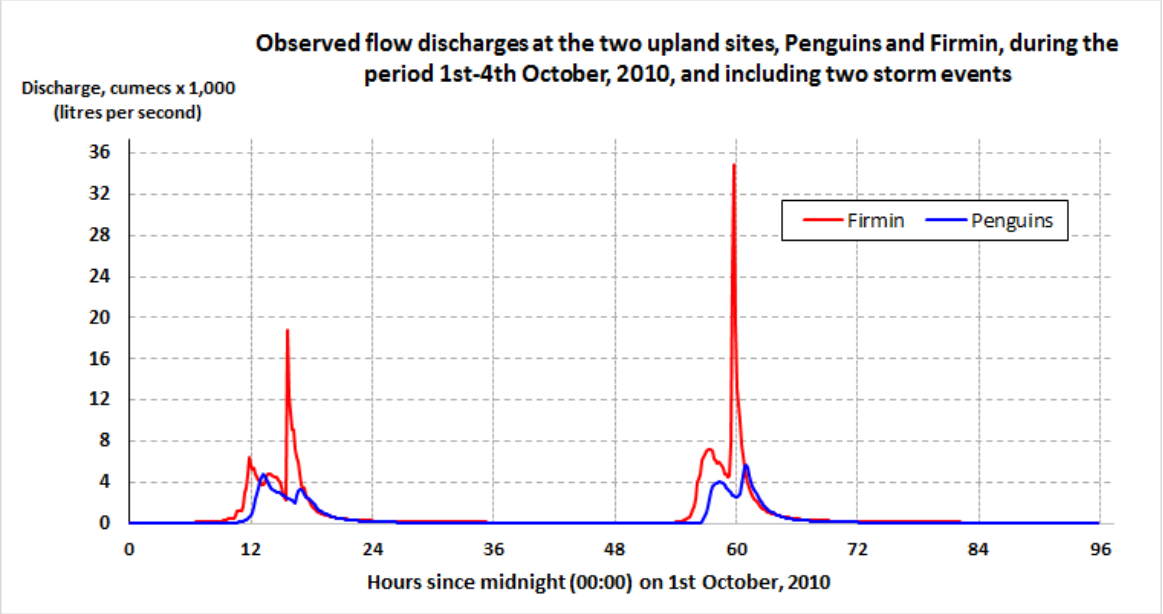

Figure 2.9: observed discharges at the two study sites, used as flow input data for the model runs.

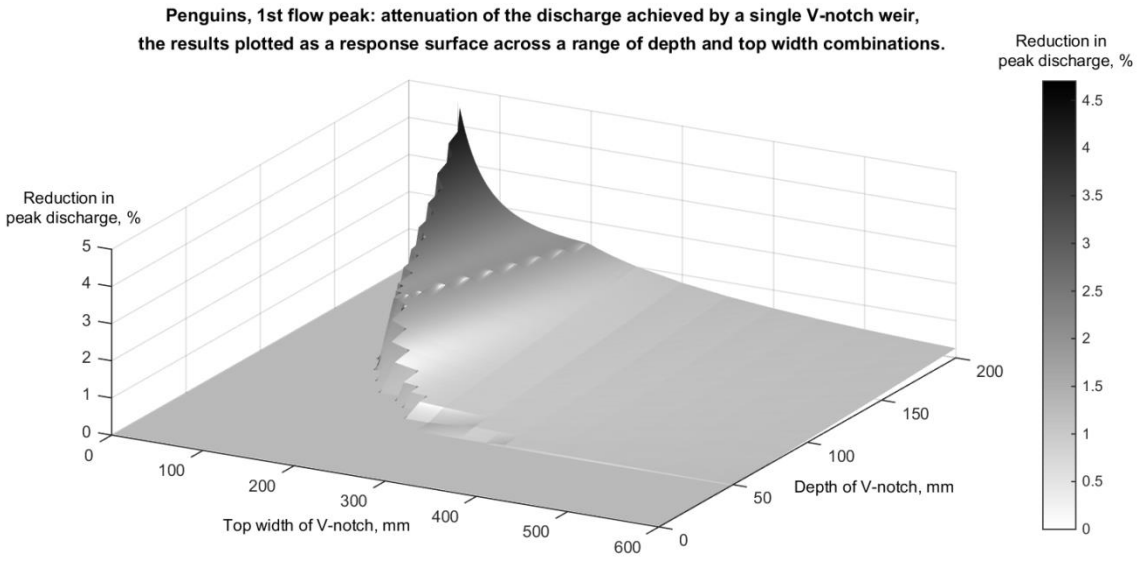

Figure 2.10: perspective view showing the effectiveness of V-notch weirs of different geometries (width and depth) in terms of the reduction in peak flow due to a single weir for storm P1.

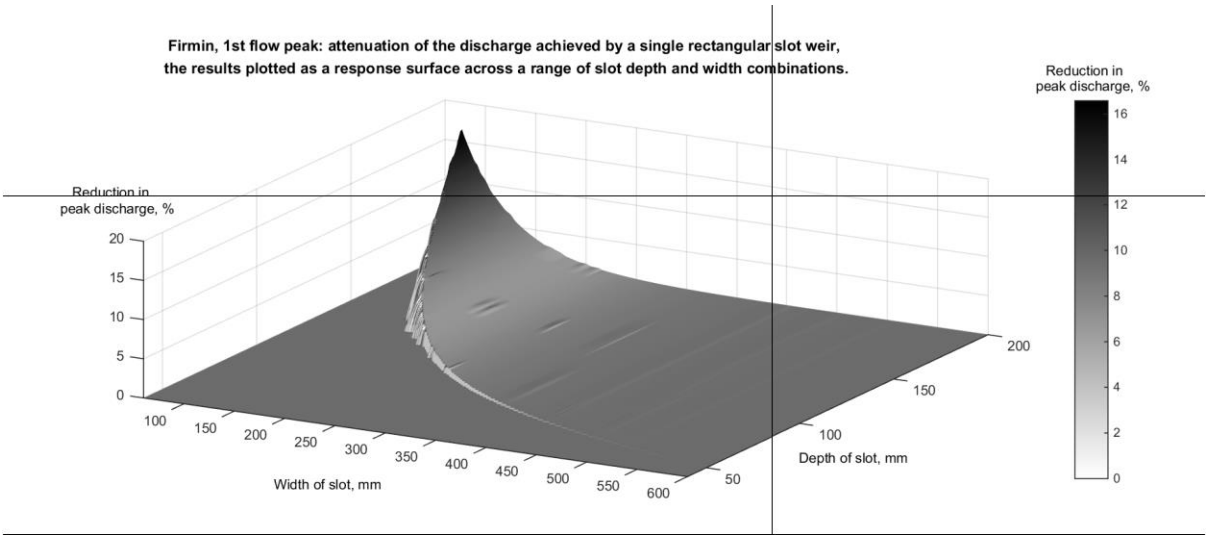

Figure 2.11: perspective view showing the effectiveness of rectangular slot weirs of different geometries (width and depth) in terms of the reduction in peak flow due to a single weir for storm P1.

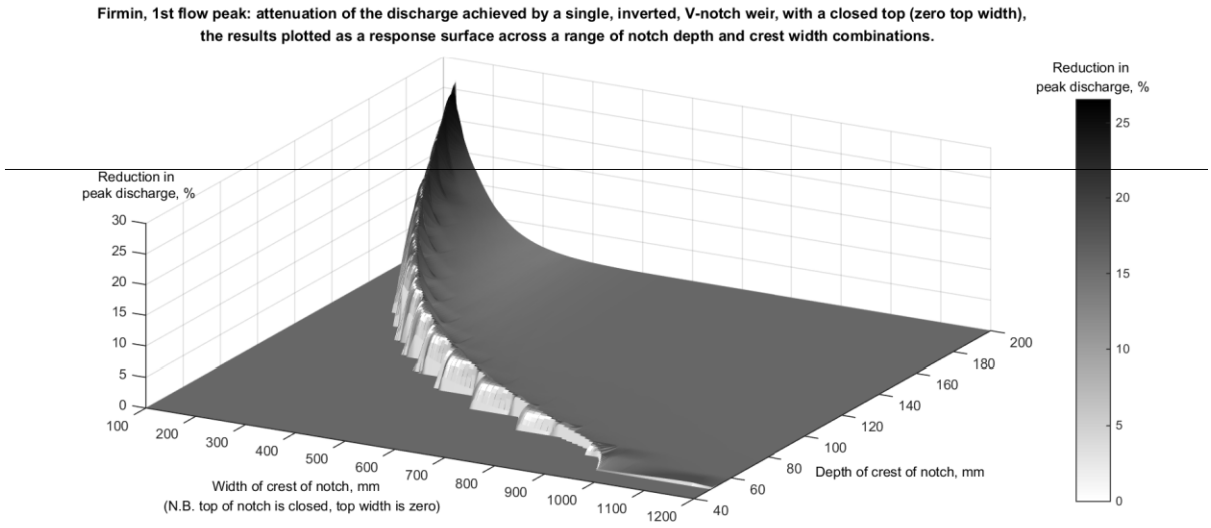

Figure 2.12: perspective view showing the effectiveness of inverted V-notch weirs of different geometries (width and depth) in terms of the reduction in peak flow due to a single weir for storm F1.

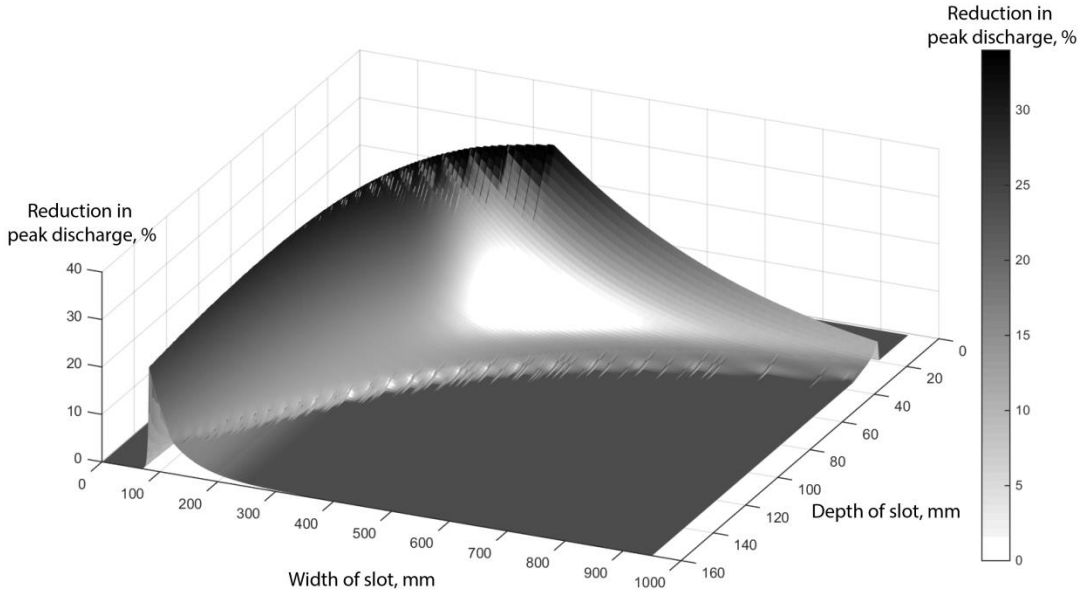

Figure 2.13: perspective view showing the effectiveness of inverted V-notch weirs of different geometries (width and depth) in terms of the reduction in peak flow due to a single weir for storm F1.

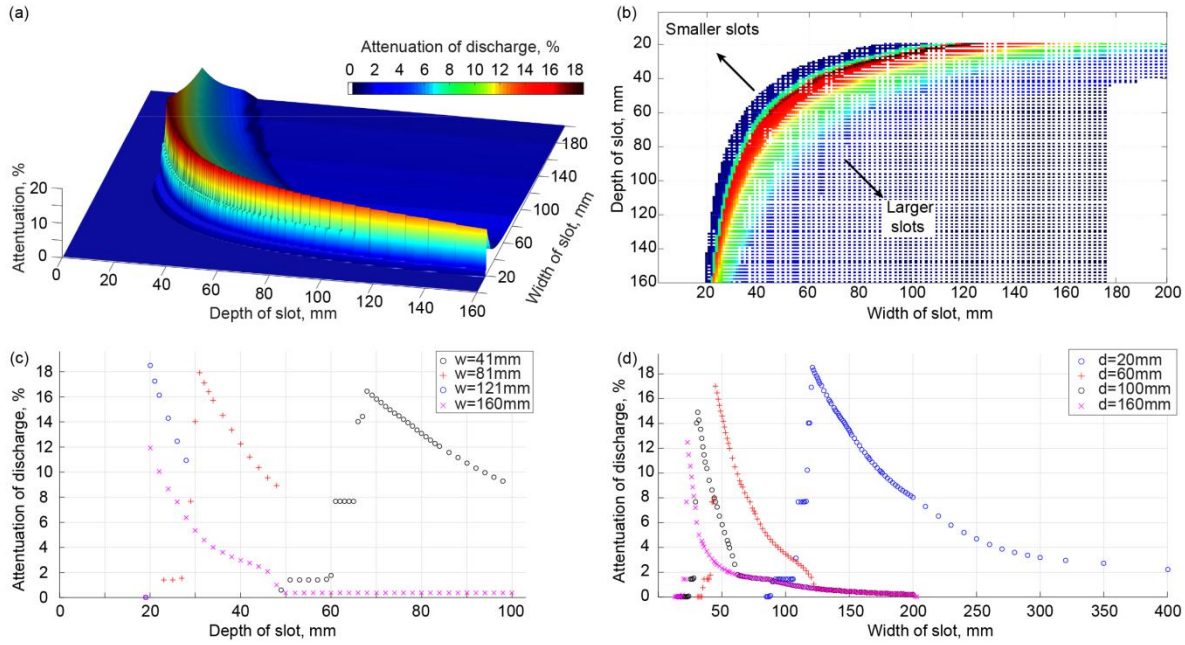

Figure 2.14: perspective (a) and plan (b) views of percentage reduction in peak flow for storm P1 for letter box slot weirs with varying slot width and depth; c) percentage reduction in peak flow with varying slot width for slots of 20, 60, 100 and 140 mm depth; c) percentage reduction in peak flow with varying slot depth for slots of 40, 80, 120 and 160 mm width. Note (c) and (d) are slices through the surface shown in (a) and (b). The base of the slot is 200mm below the top of the block, the gully is 3 m wide, and the pond upstream 7 m behind the block

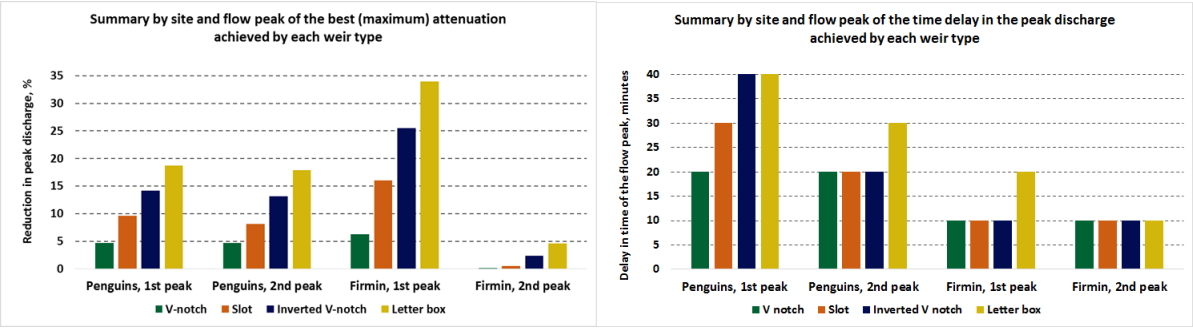

Figure 2.15: Summary of the best: a) attenuation of discharge and b) delay of peak flow achieved by each of the weir types singly for each site and flow peak. The optimised weir dimensions have been used for each peak and the crest is set to 20 cm below the brow in all cases.

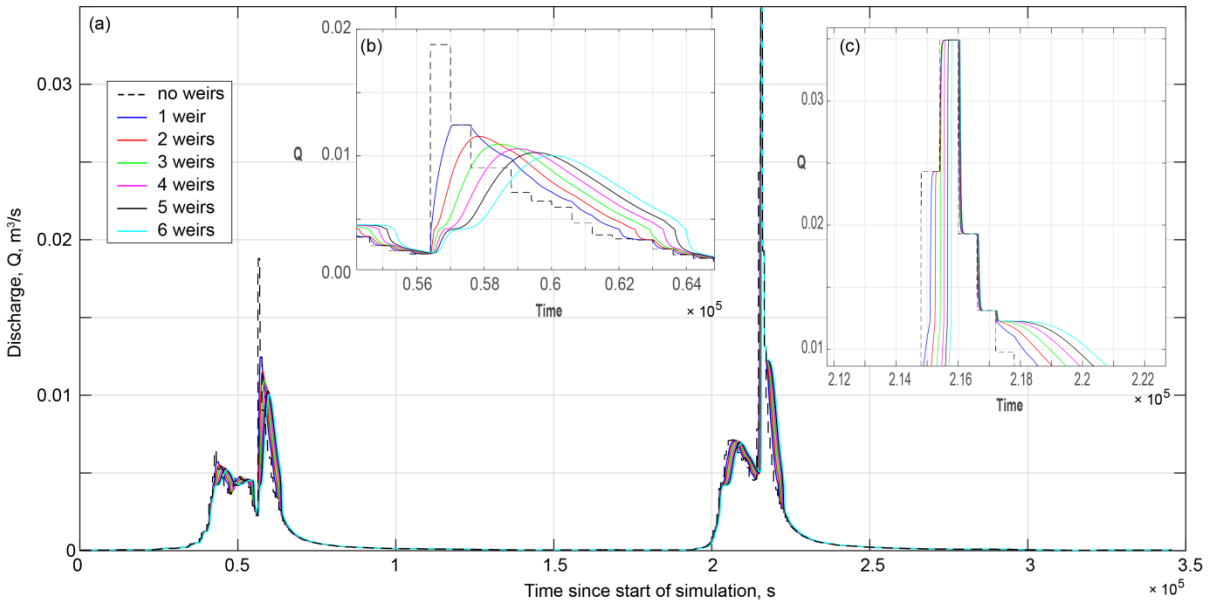

Figure: 16: Hydrographs for storms F1 and F2 downstream of a cascade of 1-6 weirs using a letterbox slot design optimised for the first storm.

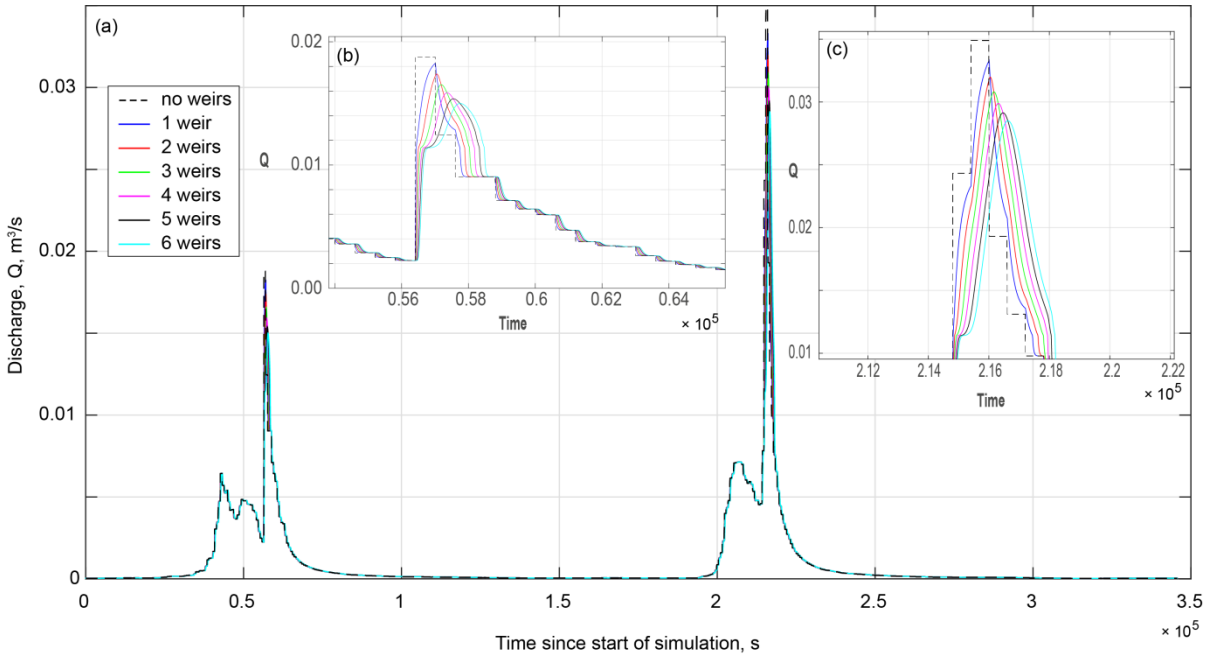

Figure: 17: Hydrographs for storms F1 and F2 downstream of a cascade of 1-6 weirs using a letterbox slot design optimised for the second storm.

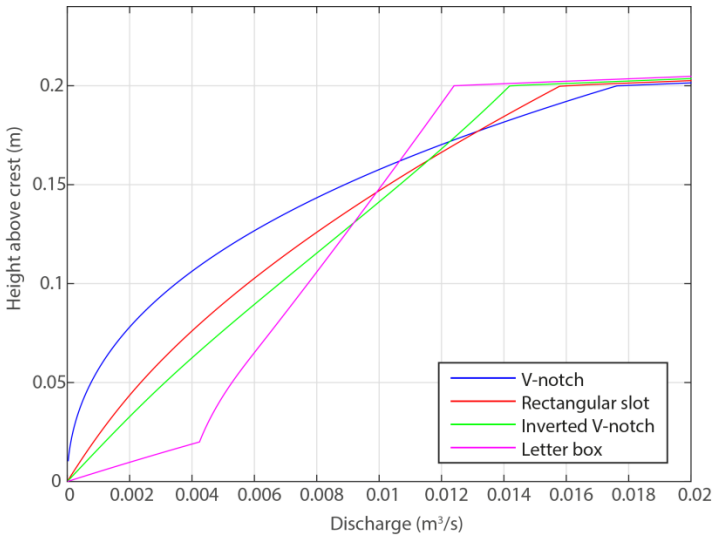

Figure 2.18: Relationship between discharge over the weir crest and height of water above the weir crest for the four weir designs optimised for storm F1. In each case the top of the weir is 0.2 m above the base of the crest explaining the sharp break in the relationship at a height of 0.2 m in each case.

Table 2.1. Summary data for the two study sites

	Penguins – site "P"	Firmin – site "F"
Area, m^2	**5,120**	**7,008**
Length, m	**190**	**160**
Max. width, m	**45**	**70**
Max. elevation, m	**514.5**	**619.0**
Min. elevation, m	**505.2**	**612.1**
Notes on condition	**Intact, no open erosion or gullying, good ground cover by vegetation, gently sloping channels or flow paths**	**Badly eroded and gullied, large areas of bare peat, steeply sloping channel banks with some overhangs, some steep channel gradients**

Table 2.2. Summary of attenuation of the peak discharges due to passing the flow through a single, V-notch weir (Figure 2.6), 20 cm deep, top width optimised to achieve the maximum attenuation. Results shown for both sites and peak discharges.

Site and peak event	First peak				Second peak			
	Discharge, cumecs		Reduction in peak, %	Delay, minutes	Discharge, cumecs		Reduction in peak, %	Delay, minutes
	Observed	Modelled			Observed	Modelled		
Penguins								
As optimised for 1st peak: d=200mm, w_{top}=54.3mm	0.00471	0.00449	4.70	20	0.00560	0.00560	0	6
As optimised for 2nd peak: d=200mm, w_{top}=64.6mm	"	0.00454	3.66	20	"	0.00534	4.72	20
Firmin								
As optimised for 1st peak: d=200mm, w_{top}=213.2mm	0.0188	0.0176	6.22	10	0.0349	0.0349	0	9
As optimised for 2nd peak: d=200mm, w_{top}=422.0mm	"	0.00185	1.28	10	"	0.0349	0.05	10

Table 2.3. Summary of attenuation of the peak discharges due to passing the flow through a single, rectangular slot weir (Figure 2.5), 20 cm deep, slot width optimised to achieve the maximum attenuation. Results shown for both sites and peak discharges.

Site and peak event	First peak				Second peak			
	Discharge, cumecs		Reduction in peak, %	Delay, minutes	Discharge, cumecs		Reduction in peak, %	Delay, minutes
	Observed	Modelled			Observed	Modelled		
Penguins								
As optimised for 1st peak: d=200mm, w_{top}=20.8mm	0.00471	0.00426	9.63	30	0.00560	0.00560	0	5
As optimised for 2nd peak: d=200mm, w_{top}=25.2mm	"	0.00434	7.73	30	"	0.00514	8.14	20
Firmin								
As optimised for 1st peak: d=200mm, w_{top}=77.2mm	0.0188	0.0158	16.0	10	0.0349	0.0349	0	6
As optimised for 2nd peak: d=200mm, w_{top}=169.7mm	"	0.0183	2.38	10	"	0.0347	0.53	10

Table 2.4. Summary of attenuation of the peak discharges due to passing the flow through a single, inverted V-notch weir (Figure 2.7), 20 cm deep, closed at the top, crest width optimised to achieve the maximum attenuation. Results shown for both sites and peak discharges.

Site and peak event	First peak				Second peak			
	Discharge, cumecs		Reduction in peak, %	Delay, minutes	Discharge, cumecs		Reduction in peak, %	Delay, minutes
	Observed	Modelled			Observed	Modelled		
Penguins								
As optimised for 1st peak: d=200mm, w_0=33.2mm	0.00471	0.00404	14.2	40	0.00560	0.00560	0	8
As optimised for 2nd peak: d=200mm, w_0=39.9mm	"	0.00424	9.89	30	"	0.00486	13.1	20
Firmin								
As optimised for 1st peak: d=200mm, w_0=116.3mm	0.0188	0.0158	25.5	10	0.0349	0.0349	0	9
As optimised for 2nd peak: d=200mm, w_0=279.6mm	"	0.0183	2.11	10	"	0.0347	2.38	10

Table 2.5. Summary of attenuation of the peak discharges due to passing the flow through a single, letter box weir (Figure 2.8), box 2 cm deep, crest set 20 cm below the brow, crest width optimised to achieve the maximum attenuation. Results shown for both sites and peak discharges.

Site and peak event	First peak				Second peak			
	Discharge, cumecs		Reduction in peak, %	Delay, minutes	Discharge, cumecs		Reduction in peak, %	Delay, minutes
	Observed	Modelled			Observed	Modelled		
Penguins								
As optimised for 1st peak: *d*=20mm, *z*=200mm, w_0=120.0mm	0.00471	0.00383	18.7	40	0.00560	0.00560	0	10
As optimised for 2nd peak: *d*=20mm, *z*=200mm, w_0=144.3mm	"	0.00403	14.3	40	"	0.00460	17.9	30
Firmin								
As optimised for 1st peak: *d*=20mm, *z*=200mm, w_0=389.0mm	0.0188	0.0124	34.0	20	0.0349	0.0349	0	7
As optimised for 2nd peak: *d*=20mm, *z*=200mm, w_0=1045mm	"	0.0183	2.78	10	"	0.0333	4.61	10

Table 2.6. Values of the coefficient *k* from eq. 11 for a range of letter box slot depths (*d*) and board heights (z_1)

Z_1\d	0.02	0.04	0.06
0.10	50.4	27.1	19.4
0.15	38.5	20.4	14.4
0.20	31.4	16.4	11.5
0.25	26.6	13.9	9.6
0.30	23.2	12.0	8.3

3 REFERENCES

Allott, T.E., Evans, M.G., Lindsay, J.L., Agnew, C.T., Freer, J.E., Jones, A. & Parnell, M. (2009). *Water tables in Peak District blanket peatlands*. Moors for the Future Report no. 17, Moors for the Future, Edale.

Bazin, H.É. (1898). Experiences nouvelles sur l'ecoulement en deversoir: executees a Dijon de 1886 a 1895. Dunod.

Du, J.K., Xie, H., Hu, Y.J., Xu, Y.P. & Xu, C.Y. (2009). Development and testing of a new storm runoff routing approach based on time variant spatially distributed travel time method. *Journal of Hydrology* **369**: 44–54.

Gao, J., Holden, J. & Kirkby, M. (2014). A distributed TOPMODEL for modelling impacts of land-cover change on river flow in upland peatland catchments." *Hydrological Processes*

Goulsbra, C.S. (2010). Monitoring the connectivity of hydrological pathways in a peatland headwater catchment. *University of Manchester*: 1–235.

Holden, J., Burt, T. P., & Cox, N. J. (2001). Macroporosity and infiltration in blanket peat: the implications of tension disc infiltrometer measurements. *Hydrological Processes*, *15*(2), 289-303.

Holden, J. & Burt, T.P. (2003). Runoff production in blanket peat covered catchments. *Water Resources Research* 39, 7, 1191.

Holden, J., Kirkby, M.J., Lane, S.N., Milledge, D.G., Brookes, C.J., Holden, V. & McDonald, A.T. (2008). Overland flow velocity and roughness properties in peatlands. *Water Resources Research* 44, W06415, doi:10.1029/2007WR006052

Horton, R.E. (1906) *Weir experiments, coefficients, and formulas*. US Government Printing Office.

Lane, S.N. & Milledge, D.G. (2012). Impacts of upland open drains upon runoff generation: a numerical assessment of catchment scale impacts. *Hydrological Processes* 27, 1701-1726.

Lindsay, J.B. (2014). The whitebox geospatial analysis tools project and open-access GIS." In *Proceedings of the GIS research UK 22nd annual conference*, pp. 16-18.

Maidment, D.R. (1993). Developing a spatially distributed unit hydrograph by using GIS. In Applications of Geographical Information Systems in Hydrology and Water Resource Management, Kpvar K, Nachtnebel H(eds). *International Association of Hydrological Sciences Special Publication 211*, 181–92.

Maidment, D.R., Olivera, F., Calver, A., Eatherall, A. & Fraczek, W. (1996). Unit hydrograph derived from a spatially distributed velocity field. *Hydrological Processes* **10**: 831–44.

Nagler, F.A. (1918). Verification of the Bazin Weir Formula by Hydro Chemical Gaugings. *Transactions of the American Society of Civil Engineers*, *83*(1), 105-156.

Odoni N.A. & Lane, S.N. (2010). Assessment of the impact of upstream land management measures on flood flows in Pickering Beck using overflow. Forestry commission Final Report.

http://www.forestry.gov.uk/pdf/stfap_final_report_appendix12_2_Apr2011.pdf/$FILE/stfap_final_report_appendix12_2_Apr2011.pdf

Olivera, F. & Maidment, D.R. (1999). Geographic information systems (GIS)-based spatially distributed model for runoff routing. *Water Resources Research* **35**: 1155–64.

Parrott, A., Brooks, W., Harmar, O., & Pygott, K. (2009). Role of rural land use management in flood and coastal risk management. *Journal of Flood Risk Management*, *2*(4), 272-284.

Pattison, I. & Lane, S.N. (2011). The link between land-use management and fluvial flood risk: A chaotic conception?. *Progress in Physical Geography*, 0309133311425398.

Saghafian, B. & Julien, P.Y. (1995). Time to equilibrium for spatially variable watersheds. *Journal of Hydrology* **172**:231–45.